Reducing compositional fluctuations facilitates artificial selection of microbial community function

Li Xie* and Wenying Shou*

Division of Basic Sciences, Fred Hutch Cancer Research Center, Seattle, USA

Abstract

Multi-species microbial communities often display functions - biochemical activities unattainable by member species alone, such as fighting pathogens or degrading wastes. Artificially selecting high community function is useful but rarely attempted. Here, we theoretically examine artificial selection of Helper-Manufacturer communities. Helpers digest Waste and generate Byproduct essential to Manufacturers; Manufacturers divert a fraction of their growth to make Product. Thus, community function - total Product accumulated as a low-density "Newborn" community grows over "maturation time" T into an "Adult" community - is costly to Manufacturers. Despite pre-optimizing Helper and Manufacturer monocultures, community function is sub-optimal. To improve community function, we simulate community selection by allowing cells in Newborn communities to grow and mutate, and select highest-functioning Adults to "reproduce" by diluting each into multiple Newborns. We find that fluctuations in Newborn composition during community reproduction (e.g. due to pipetting) can interfere with selection, and reducing fluctuations (e.g. via cell sorting) facilitates selection.

Introduction

Multi-species microbial communities often display important *functions* - biochemical activities not achievable by member species in isolation [1] [2]. For example, a six-species microbial community, but not any member species alone, cleared relapsing *Clostridium difficile* infections in mice [1]. As another example, cellulose-degrading communities often harbor non-cellulolytic aerobic bacteria which, by depleting oxygen, establish a proper anaerobic environment for cellulolytic bacteria [2].

Community functions arise from *interactions* where an individual alters the physiology of another individual. Thus, to improve community function, one could take a "bottom-up" approach by identifying and modifying interactions [3, 4]. In reality, this is no trivial task given that even two species can engage in complex interactions: each species can release tens or more compounds, many of which could influence partner species in diverse fashions [5, 6, 7, 8]. Then, from this "haystack" of interactions, we will need to identify those interactions that are critical for community function, and modify them by altering species genotypes or abiotic environment.

*Author of correspondence

[1] Community function may be defined as biochemical activities not achievable to the same extent by summing activities of member species monocultures. Our definition here is more restrictive.

[2] A community function is a community trait, but a community trait may or may not be a community function. For example, total population size is a community trait and not a community function, since individual species also has a population size. Here, we are interested in community function.

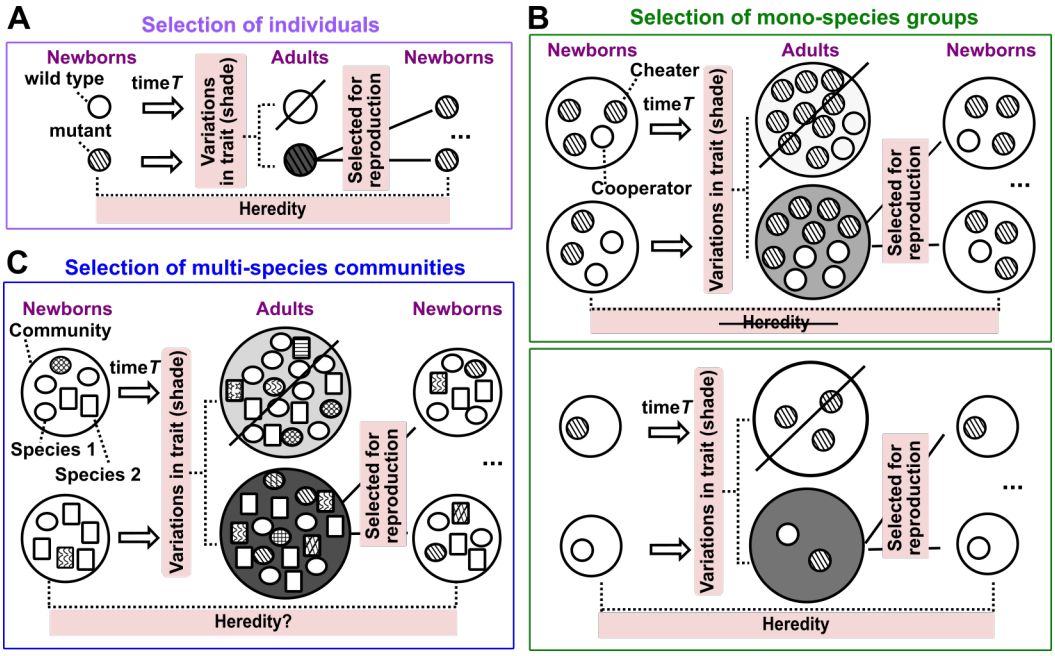

Figure 1: **Figure 1. Artificial selection can be more challenging for multi-species communities than for individuals or groups of individuals.** We consider artificial selection on a trait, where the entity under selection is an individual (**A**), a mono-species group (**B**), or a multi-species community (**C**). In each selection cycle, a population of "Newborn" entities (which can be individuals, mono-species groups, or multi-species communities) grow for a fixed maturation time T to become "Adults". Adults expressing a higher level of the desired trait (darker entity shade) are artificially selected to have a higher chance of reproduction. An individual reproduces by making copies of itself, while an Adult group or community reproduces by randomly splitting into multiple Newborns. (**A**) Artificial selection on individuals. Unlike natural selection which selects for fastest-growing cells, in artificial selection we select for traits which often impose a fitness cost to individuals (e.g. over-expression of a recombinant protein). We artificially select for individuals with desired trait and allow only these individuals to reproduce. Phenotypes are largely heritable from one generation to the next due to the constancy of genotypes, so long as mutation and recombination rates are not extraordinarily high. Artificial selection on individuals has successfully yielded improved green fluorescent protein [9], enzymes with new properties [10], and antibody fragments with high antigen-binding affinity [11]. (**B**) Artificial selection on mono-species groups. Group selection, and in a related sense, kin selection [12, 13, 14, 15, 16, 17, 18, 19, 20, 21, 22, 23, 24, 25, 26], have been extensively examined to explain, for example, the evolution of traits that lower individual fitness (e.g. sterile ants) but increase the success of a group. In this diagram, cooperators pay a fitness cost (giving rise to two instead of three offspring) to generate the product of interest (shade), while cheater mutants avoid paying the fitness cost (giving rise to three offspring) and generate no product. The trait of interest is the total amount of product in an Adult group. Artificial selection favors cooperator-dominated groups over cheater-dominated groups, although within a group, cheaters grow faster than cooperators. If Newborn groups have a large population size (**top**), then both variation and heredity are compromised: due to large size, all Newborn groups will harbor similar fractions of cheaters, thereby diminishing inter-group variations. During maturation, cheater frequency will increase, thereby diminishing heredity. In contrast, when Newborn groups are initiated at a small size such as one individual (**bottom**), a Newborn group will comprise either a cooperator or a cheater, thereby ensuring variation. Furthermore, even if cheater mutants were to arise during maturation, some Newborn groups of the next cycle will by chance inherit a cooperator, thereby ensuring some level of heredity. Thus, group selection can be effective when Newborn size is small [15, 27, 28]. (**C**) Artificial selection on multi-species communities. Since maturation time T is defined by an experimentalist, Adulthood may or may not correspond to a specific physiological state. Mechanisms that reduce heredity include: 1) changes in genotype and species abundance within a cycle due to evolution and ecological interactions, and 2) random fluctuations in Newborn composition during community reproduction.

Alternatively, one could take a "top-down" approach by artificially selecting for microbial communities exhibiting high community function. In theory, artificial selection can be applied to any population of entities. An entity can be, for example, an individual (Figure 1A), a mono-species group of individuals (Figure 1B), or a multi-species community (Figure 1C) [29]. The boundary of a group or a community is artificially imposed (e.g. in microtiter wells or fluidic droplets). Successful artificial selection requires that i) entities display trait variations; ii) trait variations can be selected to result in differential fitness in terms of entity survival and reproduction; and iii) entity trait is sufficiently heritable from one selection cycle to the next [30]. In all three types of selections, variations in a trait can be introduced by mutations and recombinations in individuals (different hatch patterns in Figure 1). Artificial selection also operates similarly among the three types of selections. Heredity is generally high when selecting for individuals (Figure 1A legend). When selecting for groups [3] , if Newborn groups have a small population size, sufficient heredity can be achieved to allow group selection to work (Figure 1B legend).

During artificial community selection, we choose a sufficiently short maturating time T so that newly-arising genotypes rarely reach high frequency within T. This way, community function is mostly determined by Newborn *composition* (the biomass of each genotype in each member species). We define *community variation* as the dissimilarity in composition among Newborn communities within a cycle, and *community heredity* as the similarity of Newborn composition from one cycle to the next [4]. Community variation and heredity are almost two opposite sides of a coin. Mutations, by creating phenotypic variations among individuals, can increase community variation and reduce community heredity. Furthermore during community reproduction, stochastic fluctuations in Newborn composition increases community variation and reduces heredity. During community maturation, genotype and species abundances can rapidly change due to ecological interactions and evolution (e.g. "cheaters" out-competing "cooperators" in Figure 1). This further compromises heredity. Thus, artificial selection of community function may be hindered by insufficient heredity.

How effective is community selection in theory and in practice? So far, community selection has been attempted only a small number of times. In simulations, multi-species communities were selected based on how community abiotic environment departed from or approached an arbitrary target [36]. Indeed, this community trait responded to community selection, and in at least some cases, the selected community trait could not be realized by single species. However, the response quickly leveled off, and was generated even without mutations. Thus, community selection likely acted on preexisting variations in community species composition. In experiments, artificial selections have been performed on complex microbial communities to improve their abilities to degrade a pollutant or support plant growth [37, 38]. Strikingly, a community trait may sometimes fail to improve despite selection, and may improve even without selection [37, 38].

Intriguing as these selection attempts might be, how they operated is unknown. First, is the trait under selection a community function or simply a trait of one member species? If the latter, then community selection is not even needed. Second, does selection act solely on species compositions or also on newly-arising genotypes? This is an important distinction because if selection acts solely on species compositions, then without immigration of new species, community function will quickly level off [36]. On the other hand, if selection acts on genotypes, then community function can potentially continue to improve as new genotypes are generated. Third, does community selection run counter to natural selection? For example, during pollutant remediation, microbes may pay a fitness cost to release a pollutant-degrading enzyme. In this case, selecting high-degradation communities would favor high-degraders, while natural selection would favor low-degraders. Alternatively, microbes may exploit pollutant as a nutrient for growth. In this case, high-degraders are also fast growers, and are favored by both natural selection and community selection. In

[3] Group selection is often applied in a broader sense to spatially-structured populations to explain the evolution of cooperative traits [31, 32]. In these cases, individuals form groups. Within each cycle, individuals grow based on their genotype (e.g. cooperators or cheaters) and group environment (cooperator-dominated or cheater-dominated). At the end of each cycle, individuals migrate among groups. However, if there are no births or deaths of groups, then selection acts on individuals instead of on groups [33, 34, 35].

[4] For any microbial community in the absence of stochasticity (e.g. mutations, stochastic death events), its dynamics starting at a given abiotic environment is determined by Newborn composition. Specifically, for a community with n species, for simplicity let's assume that each species has one quantitative phenotype. The community composition can then be specified by a set of functions $\{S_1(x_1), S_2(x_2), ..., S_n(x_n)\}$ where $S_i(x_i)$ describes the biomass distribution of the ith species over the quantitative phenotype x_i. A simple definition of the similarity between two microbial communities with compositions $\{S_1(x_1), S_2(x_2), ..., S_n(x_n)\}$ and $\{S_1^*(x_1), S_2^*(x_2), ..., S_n^*(x_n)\}$ can then be $\sum_{i=1}^{n} w_i \int \left|S_i(x_i) - S_i^*(x_i)\right| dx_i$, where $\{w_i\}$ is a set of weights.

this case, community selection may not even be necessary.

In this article, we seek a theoretical understanding of how to rapidly improve community function when natural selection tends to reduce it. In the accompanying article, we explore how selection dynamics is shaped by community function landscape and constrained by steady state species composition, and contrast different selection regimens. These theoretical insights are intended to guide future experiments.

Results

The Helper-Manufacturer community

We consider a community of two asexual microbial species that together convert Waste (such as cellulose) to a useful Product P (such as a biofuel or an anti-cancer drug). Such communities have in fact been engineered in the laboratory [39, 40, 41, 42]. In our community (Figure 2), Waste is supplied in excess. Helper H but not Manufacturer M can grow by digesting Waste. As H grows, it releases Byproduct B, which serves as the sole carbon source for Manufacturer M. Helper and Manufacturer also compete for a shared Resource R (such as reduced nitrogen). Manufacturer invests f_P fraction of its growth potential ($f_P g_M$) to make Product P, and uses the rest $(1-f_P)g_M$ for its actual biomass growth. Community function $P(T)$ is defined as the total amount of Product P accumulated when a newly-assembled "Newborn" community matures into an "Adult" community over maturation time T (Figure 4A). Thus, community function incurs a fitness cost f_P to M. Low-producing and non-producing mutants reduce community function and are more fit than high-producers, a common problem when employing engineered microbes. In Methods Section 7, we explain pathology associated with two alternative definitions of community function.

We use a stochastic, individual-based model to describe community dynamics (Methods Section 5). Each cell continuously increases its biomass at the actual growth rate (g_H for H and $(1-f_P)g_M$ for M). Biomass growth rate increases with concentration(s) of required nutrient(s) until maximal growth rate is achieved: For H which requires Resource R and waste W, since waste W is in excess, we model growth rate as a function of R using the Monod Equation (Figure 9A). For M which requires both Resource R and Byproduct B, we adopt a dual-substrate model by Mankad and Bungay (Figure 9B) due to its experimental support [43] (Figure 10). Cell biomass starts at 1, and once it grows to the division threshold of 2, the cell divides into two equal halves, thus capturing experimental observations on *E. coli* growth [44]. Our model describes the continuous dynamics of biomass increase (Figure 11), and tracks discrete cells which is important for modeling events such as mutation and death. We model cell death as occurring stochastically to individuals at a probability determined by death rate. Changes in quantities of metabolites (Resource R, Byproduct B, and Product P) are due to release and/or consumption. Throughout the text, we use H and M to respectively represent the biomass of Helper and Manufacturer, and I_H and I_M to respectively represent the integer cell number of Helper and Manufacturer. R, B, and P respectively represent the amount of Resource (in unit of $\widetilde{R}(0)$, initial Resource in Newborn), Byproduct (in unit of $\widetilde{r}_B$, the amount of Byproduct released per H biomass produced), and Product (in unit of $\widetilde{r}_P$, the amount of Product released at the cost of one M biomass). "$\sim$" marks scaling factors, and rationales of scaling can be found in Methods Section 1. At a given maturation time T and initial Resource, community function $P(T)$ depends on *Newborn composition*, which is in turn defined by initial total biomass $N(0)$, the biomass fraction of Manufacturer $\phi_M(0)$, and the relative abundance of various H and M genotypes and phenotypes (see Methods Section 1).

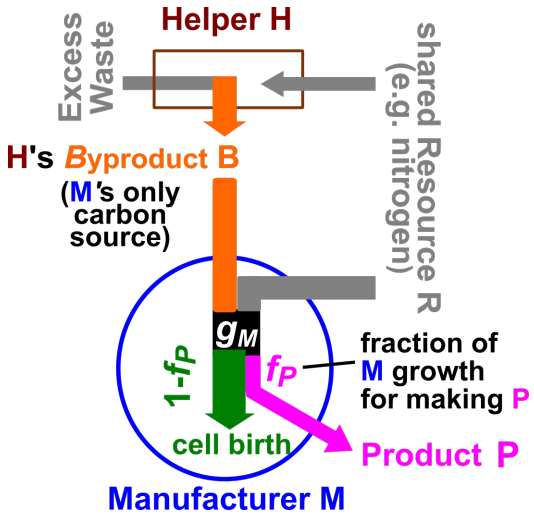

Figure 2: **Figure 2. A Helper-Manufacturer community that converts Waste to Product**. Helper H digests Waste (present in excess) to grow its biomass, and produces Byproduct B. B is the sole carbon source for Manufacturer M. M invests a fraction f_P of its potential growth g_M to make Product P, while channels the remaining $1 - f_P$ to its own biomass growth. When $f_P = 0$, M makes no Product and its growth rate is g_M; when $f_P = 1$, M uses all its resources to make Product and does not grow. H and M compete for a shared Resource R, and thus when R is depleted, cell growth stops. In this study, we assume that the release of Byproduct and Product is coupled to biomass growth.

Species coexistence in Helper-Manufacturer community

To convert Waste to Product, H and M must coexist. Coexistence can be achieved if at least one species derives a large fitness benefit (when compared to its basal fitness) from the other species [45]. In the Helper-Manufacturer community, Manufacturer obligatorily depends on Helper, and thus coexistence is possible. However, if f_P is too high (e.g. near 1), then Manufacturer will always grow slower than Helper and therefore go extinct (burgundy in the top panel of Figure 3A and in Figure 3B). At low f_P, if Byproduct from Helper allows Manufacturer to grow faster than Helper for part of a maturation cycle T, then the two species can coexist. Furthermore if species coexistence is achieved, then coexistence is stable in the sense that species ratio will converge to a steady-state value (olive and green in the bottom panel of Figure 3A and in Figure 3B).

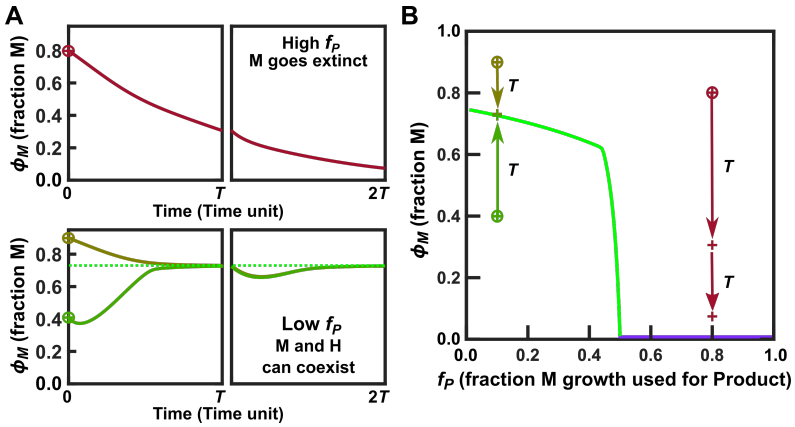

Figure 3: **Figure 3. Stable species coexistence at low f_P.** (**A**) Helper H and Manufacturer M fail to coexist when f_P is high (0.8; top). At low f_P (0.1, bottom), if M can grow faster than H for part of the maturation cycle T, then H and M can stably coexist: different initial species ratios will converge to a steady state value (dotted line). (**B**) Phase portrait showing steady state $\phi_{M,SS}$ (light green and lavender) as a function of f_P. The dynamics trajectories in **A** are re-plotted in **B**. The initial state of a Newborn community is marked with $\oplus$, and each subsequent cross ($+$) along the arrow direction represents community state at the end of a maturation cycle T. Parameters are from the last column of Table 1.

Considerations for community selection

In this section, we discuss several important considerations for community selection. First, we choose H and M phenotypes (Table 1) so that the two species can coexist for a range of f_P (Figure 3). Our parameter values are biologically feasible based on experimental measurements on microbes (details in Methods Section 2).

Second, the rate of mutations. Experimentally-measured rates of phenotype-altering mutations can vary from 10^{-8} to 10^{-3} per genome per generation depending on the phenotype of interest (e.g. a qualitative phenotype such as survival under a stress, or a quantitative phenotype such as growth rate) and a variety of other factors (Methods Section 4). Mutation rate can be further elevated by 100-fold in hyper-mutators [46, 47, 48]. Here for any mutable phenotype, we assume a high, but biologically feasible, rate of 0.002 phenotype-altering mutations per cell per generation, in part to speed up computation. When we lower mutation rate 100-fold, all of our conclusions still hold (see Figure 23).

Third, the phenotype spectrum of mutations (Methods Section 4; Figure 4B). Among phenotype-altering mutations, we assume that 50% create null mutants (e.g. maximal growth rate $g_{Species\,max} = 0$, metabolite affinity $1/K_{SpeciesMetabolite} = 0$, or $f_P = 0$), as per experimental studies on GFP, virus, and yeast [49, 50, 51]. Among not-null mutations, the fraction of mutations that enhance a phenotype ("enhancing mutations") versus those that diminish a phenotype ("diminishing mutations") is highly variable depending on, for example, effective population size and the optimality of the starting phenotype (Methods Section 4). Reasoning that a starting community is generally neither optimized nor thoroughly un-optimized, we model mutation effects based on an *S. cerevisiae* study from the Dunham lab. This study quantified the fitness effects of a large number of fitness-enhancing and fitness-diminishing mutants [52]. Our reanalysis of the Dunham lab data shows that the distribution of mutation effect is largely conserved regardless of environmental conditions (carbon-limitation, phosphate-limitation, or sulfate-limitation) or mutation types (single-copy gene deletion in haploid or diploid; extra gene copies on low-copy or high-copy plasmids in diploid) (Figure 13). In all cases, the relative fitness changes caused by fitness-enhancing and fitness-diminishing mutations can be approximated by separate exponential distributions with different means (Figure 4B). We further assume that the effects of sequential mutations are multiplicative, i.e. there is no epistasis. When we use a different distribution of mutation effect or incorporate various strengths of epistasis based on previous experimental and theoretical work (Methods Section 6; Figure 14), our conclusions still hold (see Figures 24 and 25).

Fourth, the total number of communities n_{tot}. When n_{tot} gets larger, more variations become available

for selection, but experimental setup becomes more demanding. Here, we start with a modest number of 100 Newborn communities which experimentally can be screened in 96-well plates.

Fifth, Newborn composition such as total biomass $N(0)$ and fraction of Manufacturer biomass $\phi_M(0)$. If $N(0)$ (and thus the total population size) is very large, then all communities will share similar evolutionary dynamics of accumulating and being overtaken by fast-growing, non-producing Manufacturers. This makes higher-level selection (group selection and community selection) ineffective [15, 28, 53] (Figure 1B, top). On the other hand, if $N(0)$ (and thus the total population size) is very small, then a member species could be lost by chance. Moreover, to sample rare mutations, a very large number of communities would be required. We have chosen N_0 (the target biomass of a Newborn community) to be 100 (e.g. 100 cells of biomass 1). As for species ratio, it will rapidly converge to the steady state (Figure 3) which may or may not be optimal for community function (see the accompanying article).

Sixth, maturation time T and Resource supplied to Newborn, which together determine the number of cell generations within a selection cycle. The number of generations should be sufficiently large to allow new mutations to occur, but sufficiently short because otherwise, non-producers will eventually take over all communities, reducing heredity as well as variations among communities. We choose maturation time T such that the total biomass of even evolved communities comprising fastest-growing H and M would grow from the initial ~100 biomass to at most 9.9×10^3 when $f_P = 0$, and generally to $\sim 7\times10^3$ for f_P normally encountered during community selection. At the mutation rate of 2×10^{-3} per cell per generation, a community growing from $\sim 10^2$ to $\sim 10^4$ ($\sim 6-7$ generations) samples a handful of mutations on average. We supply each Newborn community with Resource so that a maximal total biomass of 10^4 can be supported. For an average community, this choice ensures a good (~70%) usage of Resource, and the excess (30%) Resource prevents stationary phase and its physiological complications (e.g. sporulation).

Finally, community reproduction. Here, we do not allow mixing (migration) among communities to prevent non-producers from migrating to high-functioning communities. If we select a large percent of Adult communities to reproduce, then community selection is too weak. If we select a small number of Adult communities to reproduce, then variations among the next-generation Newborns could be limited. However, since we use hyper-mutators, we are not as concerned about a shortage of variations. Thus, we choose the top-functioning Adult community and reproduce it by randomly partitioning it into Newborns to achieve an average biomass of $N_0 = 100$. Since total biomass (or population size) generally increases by ~ 70 fold during maturation but we need 100 n_{tot} Newborn communities, we use the top-functioning Adult community to reproduce as many Newborns as possible, and then use the second top-functioning Adult community to generate the remaining Newborns.

To summarize (Figure 4), we start with n_{tot} of 100 Newborns. Each Newborn starts with $N(0)$ of 100 biomass units, and $H : M$ ratio converges to a steady state value (Figure 3). Each Newborn is supplied with excess Waste W and enough Resource to grow to a total biomass of 10^4. To avoid stationary phase, we choose a maturation time T so that even the fastest-growing community on average would not deplete R by the end of a selection cycle. Phenotype-altering mutations occur at a rate of 0.002 per cell per generation for each mutable phenotype (Table 1). A mutation can create a null mutant (probability = 0.5), or enhance a phenotype by an average of 5% (probability ~0.25), or diminish a phenotype by an average of 6.7% (probability ~0.25). The effects of sequential mutations are multiplicative. At the end of a cycle, Adult with the highest $P(T)$ is selected and randomly partitioned into as many Newborns as possible, and these Newborns on average have a target biomass of $N_0 = 100$. When the top-functioning Adult is exhausted, the second highest-functioning community is used until n_{tot} of 100 Newborns are generated for a new cycle. As a control, we randomly choose Adult communities to reproduce in a similar fashion.

Improving individual growth sometimes improves community function

To simulate community selection, we allow mutations to change mutable phenotypes so that phenotypes range between zero (null mutants) and respective biological upper bounds (Table 1). Mutable phenotypes include M's production parameter f_P (ranging from 0 to 1), as well as H and M's growth phenotypes (maximal growth rates and affinities for nutrients). Species phenotypes and their upper bounds are biologically reasonable (see Methods Section 2 for experimental justifications), and also allow evolved H and M to coexist for a range of f_P (Figure 3B). These mutable phenotypes have been shown to rapidly evolve (within tens to hundreds

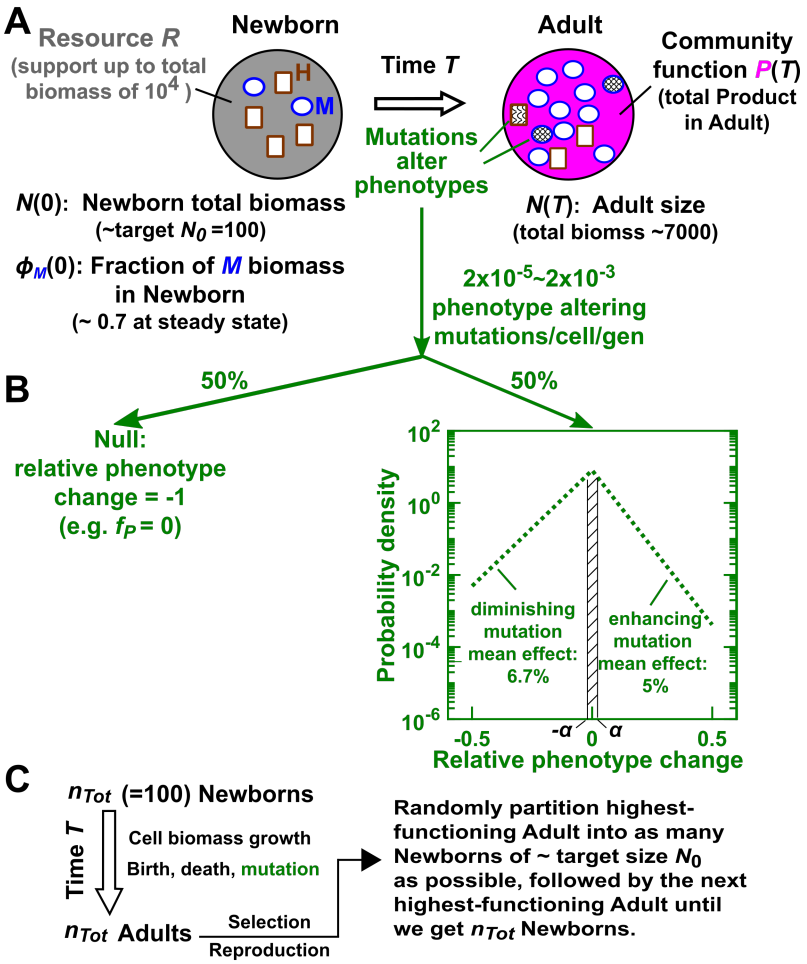

Figure 4: **Figure 4. Selection on community function.** (**A**) Definition of community function. (**B**) The distribution of relative phenotype change due to a mutation, as inferred from the Dunham lab data (see Figure 13 for full figure). For example in the case of f_P, 0.5 on the x-axis means $(f_{P,mut} - f_{P,anc})/f_{P,anc} = 0.5$. The probability of a mutation altering the relative phenotype by $\pm\alpha$ is the shaded area. See Figure 14 for how we model phenotypic effects of mutations under epistasis. (**C**) Summary of community selection simulations.

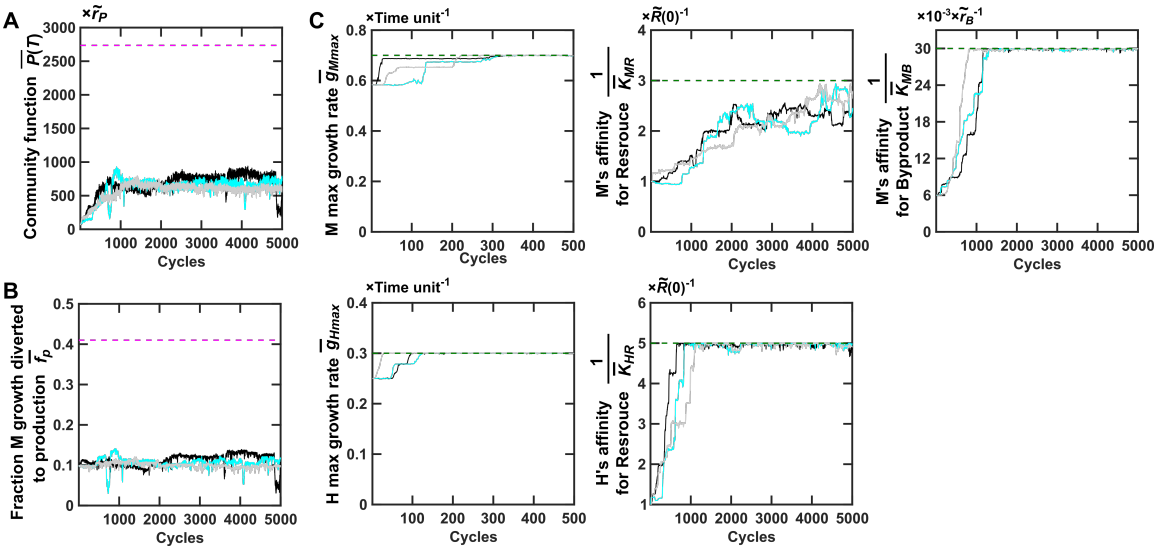

Figure 5: **Figure 5. Improved community function can be accompanied by improved individual growth.** Upon community selection, community function $P(T)$ increases (**A**). This increase is accompanied by improved individual growth (improved maximal growth rates g_{Mmax} and g_{Hmax} and affinities for metabolites $1/K_{MR}$, $1/K_{MB}$ and $1/K_{HR}$) (**C**). However, f_P increases very little (**B**). $\overline{P}(T)$ is averaged across the two selected Adult communities. $\bar{g}_{Mmax}$, $\bar{g}_{Hmax}$, and $\overline{f}_P$ are obtained by averaging within each selected Adult community and then averaging across the two selected Adults. $K_{SpeciesMetabolite}$ are averaged within each selected Adult community, then averaged across the two selected Adults, and finally inverted to represent average affinity. Green dashed lines: upper bounds of phenotypes; Magenta dashed lines: f_P optimal for community function, and maximal $P(T)$ when all five growth parameters are fixed at their upper bounds and $\phi_M(0)$ is also optimal for $P(T)$. Black, cyan, and gray curves show three independent simulations.

of generations; [54, 55, 56, 57]). We hold death rates constant because they are much smaller than growth rates and thus any changes are likely to be inconsequential. We hold consumption coefficients (c_{RH}, c_{RM}, c_{BM}) constant because the amounts of essential elements required to make biomass are unlikely to evolve dramatically due to stoichiometric constraints, especially when these elements are not supplied in large excess ([58]).

In control simulations where random communities are selected for reproduction, community function rapidly declines to zero in all replicates (Figure 15C). This is expected since in the absence of community selection, natural selection favors fast-growing non-producers ($f_P = 0$; Figure 15B). Consistent with natural selection, maximal growth rates rapidly increase to their upper bounds, and nutrient affinities also improve (Figure 15A).

When we apply community selection, community function $P(T)$ initially increases (Figure 5A). Concurrently, H and M's maximal growth rates and nutrient affinities improve toward their respective upper bounds (green dashed lines in Figure 5C). f_P does not decline, but it fails to increase even though a higher f_P would have led to a higher community function (magenta dashed lines in Figure 5A and B).

These dynamics suggest that if f_P is prevented from declining, then improving individual fitness may improve community function. Of course, this is not always true. For example, if H evolves to always grow faster than M, then H will out-compete M and community function will decline. Here, we want to fix all growth parameters (maximal growth rates and nutrient affinities) at their evolutionary upper bounds, which will allow us to simplify our model and visualize community function landscape (accompanying article). Thus, we have deliberately chosen parameters such that improving H and M's growth parameters will generally improve community function (Methods Section 3; Figures 16 and 17). Consequently, mutations that reduce growth parameters will be selected against by both natural selection and community selection. Even in the one exceptional case where M's lower affinity for R (lower $1/K_{MR}$) leads to improved M growth but lower community function when f_P is low (Figure 18), whether or not fixing the particular parameter ($1/K_{MR}$) at

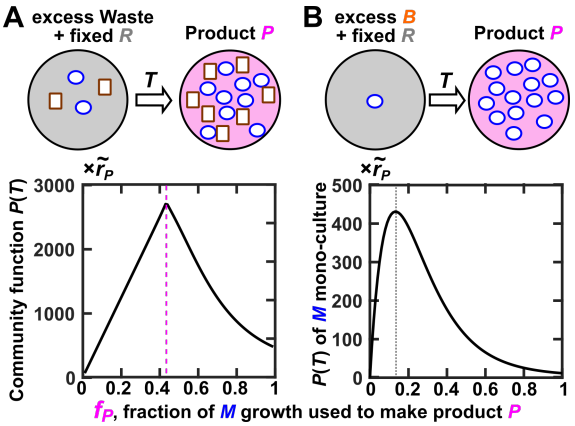

Figure 6: f_P **optimal for monoculture production may differ from** f_P **optimal for community production.** **(A)** For a Newborn H-M community supplied with a fixed Resource and excess Waste, optimal community function $P(T)$ is achieved at an intermediate $f_P^* = 0.41$ (magenta dashed line). Here the Newborn community has 60 M and 40 H cells of biomass 1, which is also the starting point of our community selection simulation. The growth parameters of M and H are all fixed at their upper bounds. **(B)** Consider a Newborn group starting with a single Manufacturer with its g_{Mmax} and $1/K_{MR}$ fixed at their upper bounds. Besides the same amount of Resource, we will need to supply Byproduct B. Experimentally, it will be difficult to supply B in a manner that mimics the community environment. If we supply excess B, maximal group function is achieved at an intermediate $f_P = 0.13$ (grey dotted line).

its upper bound does not affect community selection dynamics (Figure 26). From here on, unless otherwise stated, we fix all growth parameters at their upper bounds.

Maximal community function is achieved at an intermediate f_P

Ideally, we would like to compute global maximal $P(T)$ to test whether it can be achieved via community selection. However, given the nonlinear equations in our model (Methods Section 1), identifying global maximal can be mathematically challenging [5]. Instead, we heuristically search for a locally maximal $P(T)$ which may or may not be globally maximal but is experimentally accessible.

As discussed above, in our system we can fix all growth parameters at their upper bounds to improve community function (Methods Section 3). In this simplified scenario, for Newborn size $N(0) = 100$, we can identify f_P and $\phi_M(0)$ combination ($f_P^* = 0.41$ and $\phi_M^*(0) = 0.54$) that realizes maximal community function $P^*(T)$ (Methods, Section 8). For any $\phi_M(0)$, an intermediate f_P value maximizes community function (Figure 6A). This is not surprising: at zero f_P, no Product is made; at high f_P, Helper outcompetes Manufacturer. Importantly, the maximal $P^*(T)$ identified above cannot be further improved if we allow all growth and production parameters to mutate (Figure 19). Thus, this $P^*(T)$ is locally maximal.

f_P optimal for monoculture function may not be optimal for community function

Experimentally, how might we achieve optimal $P^*(T)$ discussed above? We can pre-adapt H via natural selection by growing H in a Resource-limited chemostat so that fastest growers dominate. If maximal growth rate and Resource affinity are independent (i.e. no trade-offs), then both will approach their upper bounds.

[5] Applied Mathematician Professor Hong Qian (University of Washington) states, "Without a closed-form solution, rigorously proving global optimum is difficult and remains an open question. Pure mathematicians may go as far as telling you the existence and uniqueness of such a solution. Applied mathematicians will forego rigor a little bit, and will come up with a "heuristic" algorithm that is usually better than brute-force parameter scans. Consequently, they can almost be sure that there is a global optimum (or not)."

For M, natural selection will yield zero f_P. Instead, we can attempt group selection to obtain high-production M monocultures. Specifically, we start with n_{tot} of 100 Newborn groups, each starting with one M cell to facilitate group selection (Figure 1B bottom panel, [27]). We supply Newborn groups with the same amount of Resource as we supply Newborn communities. Since it is difficult to reproduce community Byproduct dynamics in M monocultures, for simplicity, we supply excess Byproduct to Newborn groups. Consequently, M's affinity for B ($1/K_{MB}$) cannot be selected. When we select for high group function $P(T)$, maximal growth rate g_{Mmax} and M's affinity for Resource $1/K_{MR}$ both reach their evolutionary upper bounds, and f_P gradually increases to 0.13 (Figure 20), consistent with our calculations (Figure 6B). As expected, f_P optimal for group production occurs at an intermediate value (Figure 6B): at zero f_P , production is zero; at $f_P = 1$, M cannot grow and may even die, and thus group function is low.

To experimentally improve M's affinity for Byproduct, we can evolve ancestral M in Byproduct-limited chemostat where we expect g_{Mmax} and $1/K_{MB}$ to reach their upper bounds and f_P to decline to zero. We can then identify mutations that improve $1/K_{MB}$, and engineer them into the above group-selected M (assuming that mutations exert independent effects). We thus obtain mono-optimized M where all growth parameters are at upper bounds and f_P is optimal for M group function.

f_P optimal for group function is lower than that for community function (Figure 6) [6]. Natural selection will reduce f_P. Can we perform community selection to counter natural selection so that f_P and community function will increase?

Community function fails to improve due to non-heritable variations

Starting with Newborn communities of mono-optimized H and M, we simulate artificial community selection (Figure 4; Methods Section 5). We keep all five growth parameters fixed at their upper bounds, and only allow f_P to mutate as communities mature. We select Adult communities with the highest functions, and reproduce them by partitioning them into Newborns with target total biomass N_0 (Figure 4C). Experimentally, this is equivalent to calculating the fold-dilution by dividing $N(T)$ (the turbidity of an Adult community) by target N_0 (the target turbidity of a Newborn), and performing this dilution by pipetting a small volume of the Adult community into fresh medium (Methods Section 5). In this selection regimen, total biomass $N(0)$ and fraction of M biomass $\phi_M(0)$ fluctuate stochastically [7]. $\overline{f}_P$ barely increases and remains far below optimum (Figure 7A), similar to what we have observed earlier (Figure 5). Consequently, community function $P(T)$ also remains far below optimum (Figure 7B).

To investigate the reason for this lack of improvement, we examine correlation between $P(T)$ and Newborn composition (in terms of $\overline{f}_P(0)$, total biomass $N(0)$, and fraction of M biomass $\phi_M(0)$) during one round of selection (Figure 8). $P(T)$ should ideally depend on $\overline{f}_P(0)$ whose variations are partially heritable since Newborns sample subsets of f_P in the Adult community. However, we observe little correlation between $P(T)$ and $\overline{f}_P(0)$ (Figure 8A). For example, the Adult community displaying the highest function (left magenta dot) has a below-median $\overline{f}_P(0)$. Instead, we observe a strong correlation between $P(T)$ and $N(0)$, and between $P(T)$ and $\phi_M(0)$(Figure 8B-C).

The reason for strong correlations between $P(T)$ and $N(0)$ and between $P(T)$ and $\phi_M(0)$ becomes clear when we examine community dynamics. To minimize stationary phase, we have chosen maturation time T so that a typical community depletes the majority but not all of the Resource R. A community begins with abundant Resource and no Byproduct, so H will grow first and release Byproduct. After Byproduct has accumulated to a level comparable to M's affinity for Byproduct, M will start to grow. When a community starts with a higher-than-average $N(0)$ (dotted lines in top panels of Figure 27), M will grow to a higher biomass, deplete Resource more thoroughly, and make more Product. Similarly, if a community starts with a lower-than-average $\phi_M(0)$ (dotted lines in bottom panels of Figure 27), it will have a higher-than-average

[6] To see why this is true, we note that M grows faster in monoculture than in community, because Byproduct is in excess in monoculture whereas in community, H-supplied Byproduct is initially limiting. Thus, $\int_T g_M dt$ is larger in monoculture than in community. According to Eq. 26 (Methods Section 7), $f_P* = 1/\int_T g_M dt$ is smaller for monoculture than for community.

[7] $N(0)$ fluctuates with a standard deviation of $\sqrt{E(N(0))} = \sqrt{N_0}$. For $\phi_M(0) = M(0)/N(0)$, $\mathrm{Var}(\phi_M(0)) = \left(\frac{\mathrm{E}(M(0))}{\mathrm{E}(N(0))}\right)^2 \left[\frac{\mathrm{Var}(M(0))}{(\mathrm{E}(M(0)))^2} - 2\frac{\mathrm{Cov}(M(0),N(0))}{\mathrm{E}(M(0))\mathrm{E}(N(0))} + \frac{\mathrm{Var}(N(0))}{(\mathrm{E}(N(0)))^2}\right] = \left(\frac{N_0\phi_M(T)}{N_0}\right)^2 \left[\frac{1}{N_0\phi_M(T)} + \frac{1}{N_0}\right]$ where "E" means the expected value and "Var" means variance, and $\phi_M(T)$ is the fraction of M biomass in the Adult community from which Newborns are generated. For detailed derivation, see www.stat.cmu.edu/~hseltman/files/ratio.pdf. Thus, $\phi_M(0)$ fluctuates with a standard deviation of $\phi_M(T)\sqrt{1/\left(N_0\phi_M(T)\right) + 1/N_0}$.

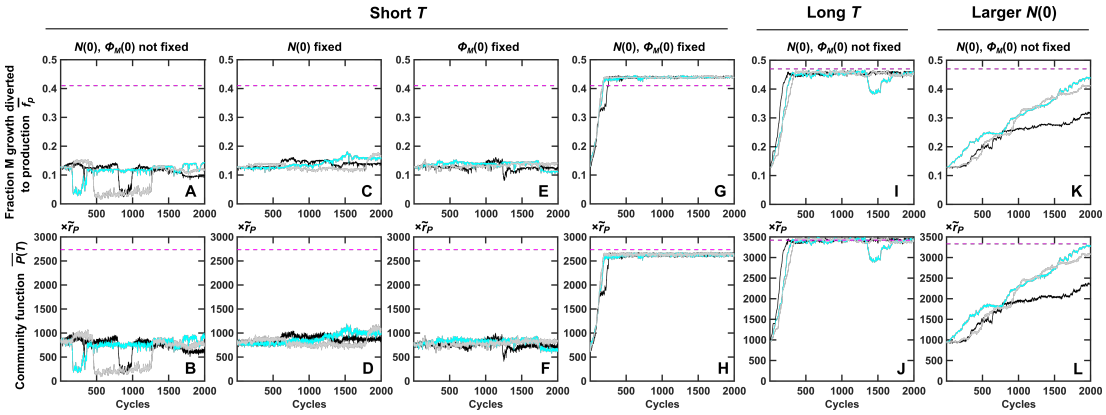

Figure 7: . **Figure 7. Evolutionary dynamics of community selection depends on how we reproduce Adult communities.** (**A-H**) Communities of mono-adapted H and M are selected for high$P(T)$ at short T (T=17, where on average the majority, but not all, Resource is consumed by the end of T to avoid stationary phase). (**A, B**) $N(0)$ and $\phi_M(0)$ are allowed to fluctuate around target total biomass of $N_0 = 100$ and $\phi_M(T)$ of the previous cycle, which is experimentally similar to diluting a volume of Adult community to fresh medium. (**G, H**) $N(0)$ and $\phi_M(0)$ are fixed to $N_0 = 100$ and $\phi_M(T)$ of the previous cycle, which is experimentally similar to sorting a fixed H and M biomass from selected Adults to Newborns. This allows community function to improve. (**C-F**) Fixing either $N(0)$ or $\phi_M(0)$ does not significantly improve community selection. (**I-L**) Communities of mono-adapted H and M are selected for high $P(T)$ at target $N_0 = 100$ and longer $T = 20$ (**I-J**), or at a larger target $N_0 = 160$ and short $T = 17$ (**K-L**). In both cases, on average Resource is depleted by the end of T. Thus, "unlucky" communities with lower $N(0)$ and/or higher $\phi_M(0)$ will have a chance to catch up. Consequently, fluctuations in $N(0)$ and $\phi_M(0)$ do not significantly affect $P(T)$, and community function improves under selection even without fixing $N(0)$ and $\phi_M(0)$. $\overline{f}_P(T)$ are obtained by averaging within each selected Adult community and then averaging across the two selected Adults. $\overline{P}(T)$ are averaged across the two selected Adults. Magenta dashed lines: f_P^* optimal for $P(T)$ and maximal $P^*(T)$ when all five growth parameters are fixed at their upper bounds and $\phi_M(0)$ is at $\phi_M^*(0)$. Black, cyan and gray curves are three independent simulations.

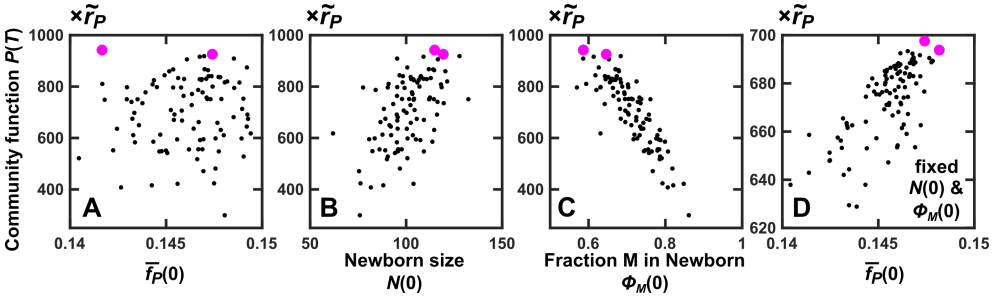

Figure 8: **Figure 8. Community function strongly correlates with Newborn total biomass and fraction of Manufacturer biomass**. (**A-C**) Nonheritable Poissonian fluctuations in $N(0)$ and $\phi_M(0)$ during community reproduction cause large variations in community function $P(T)$. In contrast, community function only weakly correlates with $\overline{f}_P(0)$, whose variations are partially heritable. Consequently, selected communities (magenta dots) may not have the highest $\overline{f}_P(0)$. (**D**) When both $N(0)$ and $\phi_M(0)$ are fixed, $P(T)$ strongly correlates with $\overline{f}_P(0)$. Each dot represents one community.

fraction of Helper. Consequently, M will endure a shorter growth lag, grow to a higher biomass, deplete Resource more thoroughly, and make more Product. Thus, random fluctuations in Newborn biomass $N(0)$ and species composition $\phi_M(0)$ during community reproduction can lead to large non-heritable variations in community function such that communities with the highest average f_P may not get selected (Figure 8A).

Reducing non-heritable variations enables community function to improve

Random fluctuations in Newborn biomass $N(0)$ and species composition $\phi_M(0)$ create non-heritable variations in community function (Figure 8). Reducing non-heritable variations should enable community selection to work. Indeed, if we fix both $N(0)$ and $\phi_M(0)$ (Methods, Section 5), equivalent to experimentally flow-sorting a fixed biomass of H and M (based on for example cell fluorescence intensity) into each Newborn, then community function becomes strongly correlated with $\overline{f}_P(0)$ (Figure 8D). Furthermore, both $\overline{f}_P$ and $P(T)$ improve (Figure 7, G and H). In this particular case, $\overline{f}_P$ overshoots f_P* and consequently, maximal $P(T)$ is not achieved (see accompanying article for an explanation). Community function improvement is not seen if either $N(0)$ or $\phi_M(0)$ is non-fixed (Figure 7, C-F). Community function also improves (Figure 22) if we distribute fixed H and M cell numbers (instead of biomass) into each Newborn community (Methods, Section 5), which can be realized experimentally by flow sorting.

Alternatively, we can reduce non-heritable variations in $P(T)$ by extending maturation time T or increasing $N(0)$ so that an average community will deplete Resource by T. In this selection regimen, Newborn communities will still experience Poissonian fluctuations in $N(0)$ and $\phi_M(0)$ during community reproduction. However, those "unlucky" communities with smaller-than-average $N(0)$ and/or larger-than-average $\phi_M(0)$ will have time to "catch up" as the "lucky" communities wait in stationary phase after exhausting Resource. Indeed, community function improves without having to fix $N(0)$ or $\phi_M(0)$ (Figure 7, **I-L**). In practice, these selection regimens will only be effective if variations in stationary phase duration introduce minimal non-heritable variations in community function.

In summary, community function improves under selection if we suppress non-heritable variations in community function. This conclusion holds when we lower the mutation rate by 100-fold (Figure 23), or use a different distribution of mutation effect (Figure 24). We have also tested the effect of epistasis (Methods, Section 6) where the effect of a mutation on f_P depends on the current f_P (Figure 14): If current f_P is high (e.g. 0.40) compared to the starting f_P (0.13, Figure 6B), then an enhancing mutation exerts a lesser effect and a diminishing mutation exerts a larger effect compared to when there is no epistasis. Conversely, if current f_P is low (e.g. $f_P = 0.04$), then the opposite is true. Under different epistasis strengths, community function improvement can be sped up by reducing non-heritable variations in $P(T)$ (Figure 25).

Discussion

How might we improve functions of multi-species microbial communities? We can enrich for the appropriate species combination. For example, using cellulose as a main carbon source enriches for communities of microbes that work together to degrade cellulose [2]. However, if we solely rely on species combinations to improve community function, then without a constant influx of new species, community function will likely stop improving [36].

Here, we consider artificial selection of communities with defined member species. The conventional wisdom may suggest "you get what you select for". But is this true? We have studied a Helper-Manufacturer community where community function is costly to Manufacturer. For community selection to be effective, we need to ensure that member species can stably coexist (Figure 3). Improving individual fitness can sometimes improve community function (Figures 5 and 17), although this often may not be true (Figure 16). Despite pre-optimizing member species in monocultures, community function may still be sub-maximal (Figure 6) due to the difficulty in recapitulating community dynamics in monocultures. Further improvements in community function can be achieved via artificial community selection, if performed properly.

Many aspects need to be taken into consideration when performing artificial community selection. It

is universally true that suppressing non-heritable variations in a trait will increase its selection efficacy. However, we show here that for community selection, large non-heritable variations in community function can readily arise via routine experimental procedures such as pipetting. For example, to avoid stationary phase, if we choose maturation time T such that Resource is in excess, then pipetting a volume of Adult community to seed a Newborn community can already introduce large, non-heritable variations in community function (Figure 8B-C). These non-heritable variations in turn partially mask heritable variations in community function caused by mutations in f_P (Figure 8A). Consequently, community function $P(T)$ remains stagnant (Figure 7A-B). In contrast, if we fix both $N(0)$ and $\phi_M(0)$ (via cell sorting for example), then community function improves (Figure 7G-H). Similarly, if we extend maturation time T or increase $N(0)$ so that Resource will on average be depleted by the end of T, then community function also improves (Figure 7I-L). However, increasing T or $N(0)$ creates variations in how much time each community spends in stationary phase, which in turn might generate non-heritable variations in community function. By the same reasoning, if Resource is in excess, then reproducing an Adult community via fixed-fold dilution (instead of diluting to a fixed total biomass or total cell number) will select for Newborn communities of larger and larger size instead of Newborn communities with higher and higher f_P (Methods, Section 9).

How does artificial selection on multi-species communities compare with artificial selection on mono-species groups? In both cases, Newborn size must not be too large and maturation time must not be too long, because otherwise, all entities will accumulate non-producers in a similar fashion. This undermines variation among entities as well as heredity of the entity trait. Community selection and group selection differ in at least two aspects. First, inter-species interactions in a community could drive species composition to a value sub-optimal for community function (accompanying article), and this problem does not exist for group-level selection [8]. Second, in group selection, when a Newborn group starts with a small number of individuals, a fraction of Newborn groups will show high similarity to the Newborn of the previous cycle (Figure 1B, bottom panel). This heredity facilitates group selection. In contrast, when a Newborn community starts with a small number of total individuals, stochastic fluctuations in Newborn community composition can be large and can interfere with community selection (Figure 7). In the extreme case, a member species can even get lost by chance. Even if a fixed number of cells from each species are sorted into Newborns, each Newborn will randomly sample a subset of genotypes in each member species. This reduces heredity and can interfere with selection [9]. If many communities are under selection, then rare communities can by chance sample a beneficial genotype from multiple species, and these beneficial genotypes rapidly rise to high frequency due to small $N(0)$. In this case, reduced heredity actually speeds up community function improvement. This bears resemblance to how sexual recombination affects evolutionary dynamics: sexual recombination reduces heredity, but when population size is large so that beneficial mutation supply is large, sexual recombination speeds up adaptation [60, 61, 62].

Microbes can coevolve with each other and with their host in nature [63, 64, 65]. This coevolution is mainly driven by natural selection. Might microbial community as a whole become a unit of selection in nature? Our work suggests that if selection for a costly microbial community function should occur in nature, then mechanisms for suppressing non-heritable variations in community function should be in place.

Methods

1 A mathematical model of the H-M community

Starting from initial conditions, the dynamics of a community comprising homogeneous H and M populations can be described by the following equations. Definitions and values of all parameters as well as definitions of scaling factors (marked by "~") are in Table 1. Definitions of variables in our model and simulations are

[8] Here, we assume that individuals in a group do not differentiate into interacting subgroups (i.e. not like cyanobacteria where some cells are photosynthetic while other cells fix nitrogen [59]).

[9] In group selection, suppose that a Newborn group starts with a single cooperator and that the highest-functioning Adult group has accumulated 80% cheaters. Then in the next cycle, 20% groups will be initiated with a single cooperator like the previous Newborn group. In community selection, suppose that a Newborn community starts with a single cooperator from each of the two species and that in the highest-functioning Adult community, each species has accumulated 80% cheaters. Then, in the next cycle, only 20%×20%= 4% communities will be initiated with pure cooperators like the previous Newborn community.

in Table 2. Variables and parameters without hats will not be scaled further. After scaling (see below for an explanation), scaling factors will become 1 and variables and parameters with hats will lose their hats.

First, M and H, the biomass of M and H, change as a function of growth and death,

$$\frac{dM}{dt} = g_M(\hat{R},\, \hat{B})\,(1 - f_P)\,M - \delta_M M \tag{1}$$

$$\frac{dH}{dt} = g_H(\hat{R})H - \delta_H H \tag{2}$$

In these equations, according to Fig 9

$$g_H(\hat{R}) = g_{Hmax}\frac{\hat{R}}{\hat{R} + \hat{K}_{HR}}$$

is the Monod growth dynamics and $g_M(\hat{R},\, \hat{B})$ takes the form of the Mankad-Bungay model [43]:

$$g_M(\hat{R},\, \hat{B}) = g_{Mmax}\frac{\hat{R}_M \hat{B}_M}{\hat{R}_M + \hat{B}_M}\left(\frac{1}{\hat{R}_M + 1} + \frac{1}{\hat{B}_M + 1}\right)$$

where $\hat{R}_M = \hat{R}/\hat{K}_{MR}$ and $\hat{B}_M = \hat{B}/\hat{K}_{MB}$.

Second, Resource $\hat{R}$ is consumed proportionally to the growth of M and H; Byproduct $\hat{B}$ is released proportionally to H growth and consumed proportionally to M growth; and Product $\hat{P}$ is released proportionally to the f_P fraction of M's growth diverted to make P.

$$\frac{d\hat{R}}{dt} = -\hat{c}_{RM} g_M(\hat{R},\, \hat{B})M - \hat{c}_{RH} g_H(\hat{R})H \tag{3}$$

$$\frac{d\hat{B}}{dt} = \widetilde{r}_B g_H(\hat{R})H - \hat{c}_{BM} g_M(\hat{R},\, \hat{B})M \tag{4}$$

$$\frac{d\hat{P}}{dt} = \widetilde{r}_P f_P g_M(\hat{R},\, \hat{B})M \tag{5}$$

Our model assumes that a fixed amount of Byproduct or Product is generated per biomass produced, which is a reasonable assumption given the stoichiometry of metabolic fluxes and has been experimentally observed [66]. Products such as secondary metabolites may be released during stationary phase, and future work will test whether variations in this assumption will change our conclusions. The initial conditions are described by total biomass $N(0) = M(0) + H(0)$, the fraction of M biomass $\phi_M(0) = M(0)/N(0)$, and the total amount of Resource supplied at the beginning of a selection cycle $\widetilde{R}(0)$. The volume of a community V is set to be 1, and thus cell or metabolite quantities (which are considered here) are numerically identical to cell or metabolite concentrations.

We scale Resource-related variable ($\hat{R}$) and parameters ($\hat{K}_{MR}$, $\hat{K}_{HR}$, $\hat{c}_{RM}$, and $\hat{c}_{RH}$) against $\widetilde{R}(0)$ (Resource supplied to Newborn), Byproduct-related variable ($\hat{B}$) and parameters ($\hat{K}_{MB}$ and $\hat{c}_{BM}$) against $\widetilde{r}_B$ (amount of Byproduct released per H biomass born), and Product-related variable ($\hat{P}$) against $\widetilde{r}_P$ (amount of Product made at the cost of one M biomass). For biologists who usually think of quantities with units, the purpose of scaling (and getting rid of units) is to reduce the number of parameters. For example, H biomass growth rate can be scaled against initial Resource $\widetilde{R}(0)$:

$$\begin{aligned} g_H(\hat{R}) &= g_{Hmax}\frac{\hat{R}}{\hat{R} + \hat{K}_{HR}} \\ &= g_{Hmax}\left(\frac{\hat{R}}{\widetilde{R}(0)}\right) \Big/ \left(\frac{\hat{R}}{\widetilde{R}(0)} + \frac{\hat{K}_{HR}}{\widetilde{R}(0)}\right) \\ &= g_{Hmax}\frac{R}{(R + K_{HR})} \\ &= g_H(R) \end{aligned}$$

where $R = \hat{R}/\widetilde{R}(0)$ and $K_{HR} = \hat{K}_{HR}/\widetilde{R}(0)$. Thus, the unscaled $g_H(\hat{R})$ and the scaled $g_H(R)$ share identical forms. The value of $\widetilde{R}(0)$ becomes irrelevant since all R-related terms are relative to $\widetilde{R}(0)$ and the initial Resource has the value of 1 with no units. Similarly, since $\hat{R}_M = \frac{\hat{R}}{\widetilde{R}(0)} \Big/ \frac{\hat{K}_{MR}}{\widetilde{R}(0)} = \frac{R}{K_{MR}} = R_M$ and $\hat{B}_M = \frac{\hat{B}}{\widetilde{r}_B} \Big/ \frac{\hat{K}_{MB}}{\widetilde{r}_B} = \frac{B}{K_{MB}} = B_M$, $g_M(\hat{R}, \hat{B}) = g_M(R, B)$. As another example, after scaling $\hat{P}$ against $\widetilde{r}_P$, we have

$$\begin{aligned} \frac{dP}{dt} &= \frac{d\hat{P}}{\widetilde{r}_P dt} \\ &= f_P g_M(\hat{R}, \hat{B}) M \\ &= f_P g_M(R, B) M \end{aligned} \tag{6}$$

and thus parameter $\widetilde{r}_P$ is no longer necessary. Other scaled equations are:

$$\begin{aligned} \frac{dR}{dt} &= \frac{d\hat{R}/\widetilde{R}(0)}{dt} \\ &= -\frac{\hat{c}_{RM}}{\widetilde{R}(0)} g_M(\hat{R}, \hat{B}) M - \frac{\hat{c}_{RH}}{\widetilde{R}(0)} g_H(\hat{R}) H \\ &= -c_{RM} g_M(R, B) M - c_{RH} g_H(R) H \end{aligned} \tag{7}$$

$$\begin{aligned} \frac{dB}{dt} &= \frac{d\hat{B}/\widetilde{r}_B}{dt} \\ &= g_H(\hat{R}) H - \frac{\hat{c}_{BM}}{\widetilde{r}_B} g_M(\hat{R}, \hat{B}) M \\ &= g_H(R) H - c_{BM} g_M(R, B) M \end{aligned} \tag{8}$$

$$\frac{dM}{dt} = g_M(R, B)\,(1 - f_P)\,M - \delta_M M \tag{9}$$

$$\frac{dH}{dt} = g_H(R) H - \delta_H H \tag{10}$$

We have not scaled time here, although time can also be scaled by, for example, the community maturation time. Here, time has the unit of unit time (e.g. hr), and to avoid repetition, we often drop the time unit.

2 Parameter choices

H can grow on Resource alone. For ancestral H, we set $g_{Hmax} = 0.25$, $K_{HR} = 1$ (i.e. K_{HR} is one unit of $\widetilde{R}(0)$) and $c_{RH} = 10^{-4}$. This way, ancestral H can grow by about 10-fold by the end of $T = 17$. These parameters are biologically realistic: time unit can be arbitrarily chosen, and if we choose hour as the unit, then g_{Hmax} translates to a doubling time of 2.8 hrs. Furthermore, for a *lys- S. cerevisiae* strain with lysine as Resource, Monod constant is $\hat{K} = 1$ μM, and consumption $\hat{c}$ is 2 fmole/cell (Ref. [67], Figure 2 Source Data 1). Thus, if we choose 20 μL as volume $\hat{V}$ and 1 μM as initial Resource concentration, then $\widetilde{R}(0) = 2 \times 10^4$ fmole. After scaling, $K = \hat{K}\hat{V}/\widetilde{R}(0) = 1$ and $c = \hat{c}/\widetilde{R}(0) = 10^{-4}$.

To ensure the coexistence of H and M, M must grow faster than H for part of the maturation cycle. Thus, i) g_{Mmax} must exceed g_{Hmax} (Figure 3) since we have assumed M and H to have the same affinity for R (Table 1); ii) M's affinity for Byproduct ($1/K_{MB}$) must be sufficiently large; and iii) Byproduct consumed per Manufacturer c_{BM} must be sufficiently small so that growth of M can be supported by H. Thus for ancestral M, we choose $g_{Mmax} = 0.58$ (equivalent to a doubling time of 1.2 hrs). We set $\hat{c}_{BM} = \frac{1}{3}$ units of r_B (i.e. $c_{BM} = \frac{1}{3}$). This means that Byproduct released during one H biomass growth is sufficient to generate 3 M biomass, which is biologically achievable ([68, 69]). When we choose $\hat{K}_{MB} = \frac{5}{3} \times 10^2$ units of

	Definition	Ancestral	Mono-adapted
$\widetilde{r}_B$	amount of released$\hat{B}$ released per H biomass born	scaling factor	no change
$\widetilde{r}_P$	amount of released $\hat{P}$ at the cost of one M biomass	scaling factor	no change
$\widetilde{R}(0)$	initial amount of Resource in Newborn	scaling factor	
f_P	fraction of M growth diverted to producing P	0.03	0.13
K_{MR}	fold of $\widetilde{R}(0)$ at which $g_{Mmax}/2$ is achieved in excess B	1	1/3*
K_{MB}	amount of $\hat{B}$ at which $g_{Mmax}/2$ is achieved in excess R, scaled against $\widetilde{r}_B$	$\frac{5}{3} \times 10^2$	$\frac{1}{3} \times 10^{2}$*
K_{HR}	fold of $\widetilde{R}(0)$ at which $g_{Hmax}/2$ is achieved	1	1/5*
g_{Mmax}	maximal biomass growth rate of M	0.58/unit time	0.7*
g_{Hmax}	maximal biomass growth rate of H	0.25/unit time	0.3*
δ_M	death rate of M	3.5×10^{-3}/unit time	no change
δ_H	death rate of H	1.5×10^{-3}/unit time	no change
c_{RM}	fraction of $\widetilde{R}(0)$ consumed per M biomass born	10^{-4}	no change
c_{RH}	fraction of $\widetilde{R}(0)$ consumed per H biomass born	10^{-4}	no change
c_{BM}	amount of $\hat{B}$ consumed per M biomass born, scaled against $\widetilde{r}_B$	$\frac{1}{3}$	no change
P_{mut}	mutation probability per cell division for each mutable phenotype	2×10^{-5}~ 2×10^{-3}	

Table 1: Parameters for ancestral and mono-adapted H and M. For maximal growth rates, * represents evolutionary upper bound. For $K_{SpeciesMetabolite}$, * represents evolutionary lower bound, which corresponds to evolutionary upper bound for Species's affinity for Metabolite ($1/K_{SpeciesMetabolite}$). In the text, we explain why we hold the remaining parameters constant during evolution.

Symbols	Definition
$M(t)$, $H(t)$	The biomass of M or H in a community at time t
$N(t) = M(t) + H(t)$	The total biomass in a community at time t
$\phi_M(t)$	The fraction of M biomass at time t
N_0	Pre-set target total biomass of Newborns during community reproduction
$I_M(t)$, $I_H(t)$	The integer number of M or H cells in a community at time t
$\varphi_M(t)$	The fraction of M individuals at time t
$L_M(t)$, $L_H(t)$	The biomass (length) of an individual M or H cell at time t, ranged between 1 and 2
$P(t)$	The amount of Product P in a community at time t, scaled by $\widetilde{r}_P$
$R(t)$	The amount of Resource R in a community at time t, scaled by $\widetilde{R}(0)$
$B(t)$	The amount of Byproduct B in a community at time t, scaled by $\widetilde{r}_B$
n_D	The integer fold of dilution when reproducing an Adult Community
n_{tot}	Total number of communities under selection
T	Community maturation time, corresponding to the duration of a selection cycle

Table 2: A summary of variables used in the simulation.

$\widetilde{r}_B$ (i.e. $K_{MB} = \frac{5}{3} \times 10^2$), H and M can coexist for a range of f_P (Figure 3). This value is realistic. For example, an evolved hypoxanthine-requiring *S. cerevisiae* strain achieved a Monod constant for hypoxanthine at 0.1 μM and a doubling time of $\tau_0 = 7$ hours when co-cultured with a hypoxanthine-overproducing strain (bioRxiv). If $\hat{V} = 20$ μL in our experiment, then $\hat{K}_{MB}/\widetilde{r}_B = \frac{5}{3} \times 10^2$ corresponds to an absolute release rate $\widetilde{r}_B = 0.1\,\mu M \times 20\mu\text{L}/(\frac{5}{3} \times 10^2) = 12$ fmole per cell biomass born = 12 fmole/(1 cell$\times$7 hr)$\approx$ 1.7 fmole/cell/hr, which is of the same order of magnitude as that for a lysine-overproducing yeast strain (up to 0.8 fmole/cell/hr, bioRxiv) and a leucine-overproducing strain (4.2 fmole/cell/hr [69]). Death rates δ_H and δ_M are chosen to be 0.5% of the upper bound of maximal growth rate, which is within the ballpark of experimental observations (e.g. the death rate of a *lys-* strain in lysine-limited chemostat is 0.4% of maximal growth rate, bioRxiv).

Since the biomass of various microbes share similar compositions of elements such as carbon or nitrogen [58], we assume that H and M consume the same amount of R per new cell ($c_{RH} = c_{RM}$). Since $c_{RH} = c_{RM} = 10^{-4}$ after scaling against $\widetilde{R}(0)$, the maximum yield is 10^4 biomass.

Growth parameters (maximal growth rates g_{Mmax} and g_{Hmax} and affinities for nutrients $1/K_{MR}$, $1/K_{MB}$, and $1/K_{HR}$) and production parameter ($f_P \in [0, 1]$) are allowed to change during evolution, since these phenotypes have been observed to rapidly evolve within tens to hundreds of generations ([54, 55, 56, 57]). For example, several-fold improvement in nutrient affinity [55] and ~20% increase in maximal growth rate [57] have been observed in experimental evolution. Thus we allow affinities $1/K_{MR}$, $1/K_{HR}$, and $1/K_{MB}$ to increase by 3-fold, 5-fold, and 5-fold respectively, and allow g_{Hmax} and g_{Mmax} to increase by ~20%. These bounds also ensure that evolved H and M can coexist for $f_p < 0.5$ (Figure 3B), and that Resource is on average not depleted by T to avoid cells entering stationary phase. Although maximal growth rate and nutrient affinity can sometimes show trade-off (e.g. [55]), for simplicity we assume here that they are independent of each other. We hold metabolite consumption (c_{RM}, c_{BM}, c_{RH}) constant because conversion of essential elements such as carbon and nitrogen into biomass is unlikely to evolve quickly and dramatically, especially when these elements are not in large excess ([58]). Similarly, we hold the scaling factors $\widetilde{r}_P$ and $\widetilde{r}_B$ constant, assuming that they do not change rapidly during evolution due to stoichiometric constraints of biochemical reactions. We hold death rates (δ_M, δ_H) constant because they are much smaller than growth rates in general and thus any changes are likely inconsequential.

3 Choosing growth parameters to simplify evolutionary modeling

Besides considerations in Section 1, we want to choose growth parameters so that improved cell growth (maximal growth rates and affinity for metabolites) improves community function. This way, we can assemble Newborn communities using mono-adapted H and M where all growth parameters are fixed at their respective evolutionary upper- bounds (which can be achieved via natural selection), while only allowing f_P to evolve. This simplifies our problem. As we will see in the accompanying article, this also enables us to visualize the community function landscape. It is important to note that improving individual growth does not always lead to improved community function (Figure 16).

We have chosen such a set of growth parameters and their evolutionary upper bounds. Let's first consider the case where $f_P = 0.41$, which corresponds to optimal community function (magenta dashed lines in Figure 5 and Figure 6A). If we fix four of the five growth parameters to their upper bounds, then as the remaining growth parameter improves, both individual fitness and community function increase (magenta lines in Figure 17). Thus, if community function is already optimized, then deviations from growth parameter upper bounds are disfavored by both community selection and natural selection, and hence growth parameters are naturally fixed.

Now let's consider the case where $f_P = 0.13$, which is optimal for M-monoculture function (grey dotted line in Figure 6B) and thus our starting point for community selection. Community function and individual fitness generally increase as growth parameters improve (black dashed line in Figure 17 A-D and F-I). However, at lower f_P (e.g. 0.13 corresponding to black dashed line in Figure 17 J and 0.1 corresponding to black solid line in Figure 18 A), individual fitness declines slightly when M's affinity for Resource ($1/K_{MR}$) improves. This is equivalent to decreased affinity for the abundant nutrient improving growth rate. Transporter competition for membrane space [70] could lead to this result, since reduced affinity for abundant nutrient may increase affinity for rare nutrient.

Mathematically speaking, this is a consequence of the Mankad-Bungay model [43] (Figure 10 B). Let $\mathring{S}_1 = S_1/K_1$ and $\mathring{S}_2 = S_2/K_2$. Then,

$$\begin{aligned}\frac{\partial g}{\partial K_1} &= \frac{\partial g}{\partial \mathring{S}_1}\frac{\partial \mathring{S}_1}{\partial K_1} = \frac{\partial\left[g_{max}\frac{\mathring{S}_1\mathring{S}_2}{\mathring{S}_1+\mathring{S}_2}\left(\frac{1}{1+\mathring{S}_1}+\frac{1}{1+\mathring{S}_2}\right)\right]}{\partial \mathring{S}_1}\frac{\partial \mathring{S}_1}{\partial K_1} \\ &= g_{max}\frac{\mathring{S}_1\mathring{S}_2}{(\mathring{S}_1+\mathring{S}_2)K_1}\left(\frac{\mathring{S}_1}{(1+\mathring{S}_1)^2}-\frac{\mathring{S}_2}{\mathring{S}_1+\mathring{S}_2}\left(\frac{1}{1+\mathring{S}_1}+\frac{1}{1+\mathring{S}_2}\right)\right)\end{aligned}$$

If $\mathring{S}_1 \ll 1 \ll \mathring{S}_2$ (corresponding to limiting S_1 and abundant S_2),

$$\frac{\mathring{S}_1}{(1+\mathring{S}_1)^2}-\frac{\mathring{S}_2}{\mathring{S}_1+\mathring{S}_2}\left(\frac{1}{1+\mathring{S}_1}+\frac{1}{1+\mathring{S}_2}\right) \approx \frac{\mathring{S}_1}{(1+\mathring{S}_1)^2}-\frac{1}{1+\mathring{S}_1} = -\frac{1}{(1+\mathring{S}_1)^2} \tag{11}$$

and thus $\partial g/\partial K_1 < 0$. This is the familiar case where growth rate increases as the Monod constant decreases (i.e. affinity increases). However, if $\mathring{S}_2 \ll 1 \ll \mathring{S}_1$

$$\frac{\mathring{S}_1}{(1+\mathring{S}_1)^2}-\frac{\mathring{S}_2}{\mathring{S}_1+\mathring{S}_2}\left(\frac{1}{1+\mathring{S}_1}+\frac{1}{1+\mathring{S}_2}\right) \approx \frac{1}{\mathring{S}_1}-\frac{\mathring{S}_2}{\mathring{S}_1}\frac{1}{1+\mathring{S}_2} = \frac{1}{\mathring{S}_1(1+\mathring{S}_2)} \tag{12}$$

and thus $\partial g/\partial K_1 > 0$. In this case, the growth rate decrease as the Monod constant decreases (i.e. affinity increases).

In the case of M, let S_1 represent R and let S_2 represent B. Thus, K_1 corresponds to K_{MR} and K_2 corresponds to K_{MB}. At the beginning of each cycle, R is abundant and B is limiting (Eq. 12). Thus M cells with lower affinity for R (higher K_{MR}) will grow faster than those with higher affinity (Figure 18). At the end of each cycle, the opposite is true (Figure 18). As f_P decreases, M has the capacity to grow faster and the first stage becomes more important. Thus in the Mankad & Bungay model at low f_P, M can gain higher overall fitness by lowering affinity for R (Figure 18).

Regardless, the decline in individual fitness is very slight and only occurs at low f_P at the beginning of community selection, and thus may be neglected. Indeed, if we start all growth parameters at their upper bounds, and perform community selection while allowing all parameters to vary (Figure 21), then M's affinity for Resource ($1/K_{MR}$) decreases somewhat, yet the dynamics of f_P is similar to when we only allow f_P to change (compare Figure 21D with Figure 7A). Indeed, allowing both f_P and $1/K_{MR}$ to evolve does not change our conclusions as shown in Figure 26.

4 Mutation rate and phenotype spectrum

Among mutations, a fraction will be phenotypically neutral in that they do not affect the phenotype of interest. For example, the vast majority of synonymous mutations are neutral [71]. Experimentally, the fraction of neutral mutations is difficult to determine. Consider organismal fitness as the phenotype of interest. Whether a mutation is neutral or not can vary as a function of effective population size, and selection condition. For example, at low population size due to drift, a beneficial or deleterious mutation may not be selected for or selected against, and is thus neutral with respect to selection [72, 73]. In addition, mutations in an antibiotic-degrading gene can be neutral under low antibiotic concentrations, but deleterious under high antibiotic concentrations [74]. When considering single mutations, a larger fraction of neutral mutations is mathematically equivalent to a lower mutation rate. Here on, our "mutation rate" refers to the rate of mutations that either enhance a phenotype ("enhancing mutations") or diminish a phenotype ("diminishing mutations"). For five of the mutable phenotypes in our model, enhancing mutations of maximal growth rate (g_{Hmax} and g_{Mmax}) and of nutrient affinity ($1/K_{HR}$, $1/K_{MR}$, $1/K_{MB}$) enhance individual fitness (beneficial mutations). In contrast, enhancing mutations in f_p diminish individual fitness (deleterious mutations).

Depending on phenotype, the rate of phenotype-altering mutations is highly variable. Mutations that cause qualitative phenotypic changes (e.g. canavanine or 5-fluoroorotic acid resistance) occur at a rate of 10^{-8}~10^{-6} per genome per generation in bacteria and yeast [75, 76]. Mutations affecting quantitative traits

such as growth rate occur much more frequently. For example in yeast, mutations that increase growth rate by $\geq 2\%$ occur at a rate of $\sim 10^{-4}$ per genome per generation (calculated from Figure 3 of [77]), and deleterious mutations occurs at a rate of $10^{-4} \sim 10^{-3}$ per genome per generation [51, 48]. If the phenotype of interest encompasses growth rates in diverse abiotic environments, then most of single-gene deletion mutations in *S. cerevisiae* alter phenotypes [78]. Moreover, mutation rate can be elevated by as much as 100-fold in hyper-mutators [46, 47, 48]. Here, we assume a high, but biologically feasible, rate of 0.002 phenotype-altering mutations per genome per generation to speed up computation. We have also tried 100-fold lower mutation rate. As expected, evolutionary dynamics slows down, but all of our conclusions still hold (Figure 23).

Among phenotype-altering mutations, tens of percent create null mutants, as illustrated by experimental studies on protein, virus, and yeast [49, 50, 51]. Thus, we assume that 50% phenotype-altering mutations are null (i.e. $g_{Species\,max} = 0$, or $K_{SpeciesMetabolite} = \infty$, or $f_p = 0$). Among non-null mutations, the relative abundances of enhancing versus diminishing mutations are highly variable in different experiments. It can be impacted by effective population size. For example, with a large effective population size, the survival rate of beneficial mutations is 1000-fold lower due to clonal interference (competition between beneficial mutations) [79]. The relative abundance of enhancing versus diminishing mutations also strongly depends on the optimality of the starting phenotype [49, 74, 72]. For example with ampicillin as a substrate, the TEM-1 β-lactamase acts as a "perfect" enzyme. Consequently, mutations were either neutral or diminishing, and few enhanced enzyme activity [74]. In contrast with a novel substrate such as cefotaxime, the enzyme has undetectable activity. Thus, diminishing mutations were not detected and 2% of tested mutations were enhancing [74].

Phenotypes of the ancestral community members are generally not so extreme that mutations are solely diminishing or solely enhancing. Thus, we base our model on experimental studies where a large number of enhancing and diminishing mutants have been quantified in an unbiased fashion. An example is a study from the Dunham lab where the fitness effects of thousands of *S. cerevisiae* mutations were quantified under various nutrient limitations [52].

Specifically for each nutrient limitation, the authors first measured $\triangle s_{WT} = (w_{WT} - \bar{w}_{WT})/\bar{w}_{WT} = w_{WT}/\bar{w}_{WT} - 1$, the deviation in relative fitness of thousands of bar-coded wild-type control strains from the mean fitness. Due to experimental noise, $\triangle s_{WT}$ is distributed with zero mean and non-zero variance. Then, the authors measured thousands of $\triangle s_{MT}$, each corresponding to the relative fitness change of a bar-coded mutant strain with respect to the mean of wild-type fitness (i.e. $\triangle s_{MT} = (w_{MT} - \bar{w}_{WT})/\bar{w}_{WT}$). From these two distributions, we derive $\mu_{\Delta s}$, the probability density function (PDF) of mutation fitness effect $\Delta s = \triangle s_{MT} - \triangle s_{WT}$ (see Figure 13A for an explanation), in the following manner.

First, we calculate $\mu_m(\triangle s_{MT})$, discrete PDF of mutant strain relative fitness change, with bin width 0.04. In other words, $\mu_m(\triangle s_{MT})$ =counts in the bin of $[\triangle s_{MT} - 0.02, \triangle s_{MT} + 0.02]$ / total counts/0.04 where $\triangle s_{MT}$ ranges from -0.6 and 0.6 which is sufficient to cover the range of experimental outcome. The Poissonian uncertainty of μ_m is $\delta\mu_m(\triangle s_{MT}) = \sqrt{\text{counts per bin}}/\text{total counts}/0.04$. Repeating this process for wild-type collection, we obtain PDF of wild-type strain relative fitness $\mu_w(\triangle s_{WT})$. Next, from wild type $\mu_w(\triangle s_{WT})$ and each $\mu_m(\triangle s_{MT})$, we derive $\mu_{\Delta s}(\Delta s)$, the PDF of Δs with bin width 0.04:

$$\mu_{\Delta s}(\Delta s = i \times 0.04) = 0.04 \times \sum_{j=-\infty}^{+\infty} \mu_w(j \times 0.04)\mu_m((i+j) \times 0.04). \tag{13}$$

assuming that $\triangle s_{MT}$ and $\triangle s_{WT}$ are independent from each other. Here, i is an integer from -15 to 15. The uncertainty for $\mu_{\Delta s}$ is calculated by propagation of error. That is, if f is a function of x_i (i = 1, 2, ..., n). Then s_f, the error of f, is $s_f^2 = \sum \left(\frac{\partial f}{\partial x_i} s_{x_i}\right)^2$ where s_{x_i} is the error or uncertainty of x_i. Thus,

$$\delta\mu_{\Delta s}(i) = 0.04 \times \sqrt{\sum_j \left[(\delta\mu_w(j)\mu_m(i+j))^2 + (\mu_w(j)\delta\mu_m(i+j))^2\right]} \tag{14}$$

where $\mu_w(j)$ is short-hand notation for $\mu_w(\triangle s_{WT} = j \times 0.04)$ and so on. Our calculated $\mu_{\Delta s}(\Delta s)$ with error bar of $\delta\mu_{\Delta s}$ is shown in Figure 13B.

Our reanalysis demonstrates that distributions of mutation fitness effects $\mu_{\Delta s}(\Delta s)$ are largely conserved regardless of nutrient conditions and mutation types (Figure 13B). In all cases, the relative fitness changes

caused by beneficial (fitness-enhancing) and deleterious (fitness-diminishing) mutations can be approximated by separate exponential distributions with different means s_+ and s_-, respectively. After normalization to have a total probability of 1, we have:

$$\mu_{\Delta s}(\Delta s) = \begin{cases} \frac{1}{s_+ + s_-(1-\exp(-1/s_-))} \exp(-\Delta s/s_+) & \text{if } \Delta s \geq 0 \\ \frac{1}{s_+ + s_-(1-\exp(-1/s_-))} \exp(\Delta s/s_-) & \text{if } -1 < \Delta s < 0 \end{cases} \quad (15)$$

We fit the Dunham lab haploid data (since microbes are often haploid) to Eq. 15, using $\mu_{\Delta s}(i)/\delta\mu_{\Delta s}(i)$ as the weight for non-linear least squared regression (green lines in Figure 13B). We obtain $s_+ = 0.050 \pm 0.002$ and $s_- = 0.067 \pm 0.003$.

Interestingly, exponential distribution described the fitness effects of deleterious mutations in an RNA virus significantly well [49]. Based on extreme value theory, the fitness effects of beneficial mutations are predicted to follow an exponential distribution [80, 81], which has gained experimental support from bacterium and virus [82, 83, 84] (although see [85, 77] for counter examples). Evolutionary models based on exponential distributions of fitness effects have shown good agreements with experimental data [79, 86].

We have also tried smaller average mutational effects based on measurements of spontaneous or chemically-induced (instead of deletion) mutations. For example, the fitness effects of nonlethal deleterious mutations in *S. cerevisiae* are mostly 1%~5% [51], and the mean selection coefficient of beneficial mutations in *E. coli* was 1%∼2% [82, 79]. Thus, as an alternative, we choose $s_+ = 0.02$; $s_- = -0.02$, and obtain similar conclusions (Figure 24).

5 Simulation code of community selection cycle

In our simulation, cell mutation, cell death, and community reproduction are stochastic. All other processes (biomass growth, cell division, and changes in chemical concentrations) are deterministic.

The code starts with a total of $n_{tot} = 100$ Newborn communities with identical configuration:

- each community has 100 total cells of biomass 1. Thus, total biomass $N(0) = 100$.
- 40 cells are H. 60 cells are M with identical f_P. Thus, $M(0) = 60$ and $\phi_M(0) = 0.6$.

In the beginning, a random number is used to seed the random number generator for each Newborn community, and this number is saved so that the sequence of random numbers used below can be exactly repeated for subsequent data analysis. The initial amount of Resource is 1 unit of $\widetilde{R}(0)$, and the initial Byproduct is $B(0) = 0$. The cycle time is divided into time steps of $\Delta\tau = 0.05$.

Below, we describe in detail what happens during each step of $\Delta\tau$. During an interval $[\tau,\ \tau + \Delta\tau]$, biomass growth is continuous but birth and death are discrete. Death and Product release are calculated at the end of each $\Delta\tau$. Resource $R(t)$ and Byproduct $B(t)$ between $[\tau,\ \tau + \Delta\tau]$ are calculated by solving the following equations between $[\tau, \tau + \Delta\tau]$ with the initial condition $R(\tau)$ and $B(\tau)$ using the ode23s solver in Matlab:

$$\frac{dR}{dt} = -c_{RM} g_M(R,\ B) M(\tau) - c_{RH} g_H(R) H(\tau) \quad (16)$$

$$\frac{dB}{dt} = g_H(R) H(\tau) - c_{BM} g_M(R,\ B) M(\tau) \quad (17)$$

where $M(\tau)$ and $H(\tau)$ are the biomass of M and H at time τ, respectively. The solutions from Eq. 16 and 17 are used in the integrals below.

We track the phenotypes of every H and M cell which are rod-shaped organisms of a fixed diameter. Let the biomass (length) of an H cell be $L_H(\tau)$. The continuous growth of L_H during τ and $\tau + \Delta\tau$ can be described as

$$\frac{dL_H}{dt} = g_H(R) L_H$$

thus $L_H(\tau + \Delta\tau)$ is

$$\ln \frac{L_H(\tau + \Delta\tau)}{L_H(\tau)} = \int_{\tau}^{\tau+\Delta\tau} g_H(R)dt$$

and

$$L_H(\tau + \Delta\tau) = L_H(\tau) \exp\left(\int_{\tau}^{\tau+\Delta\tau} g_H(R)dt\right). \tag{18}$$

Similarly, let the length of an M cell be $L_M(\tau)$. The continuous growth of M can be described as

$$\frac{dL_M}{dt} = (1 - f_P)g_M(R, B)L_M.$$

Thus during the interval $[\tau, \tau + \Delta\tau]$,

$$\ln \frac{L_M(\tau + \Delta\tau)}{L_M(\tau)} = \int_{\tau}^{\tau+\Delta\tau} (1 - f_P)g_M(R, B)dt$$

Thus for an M cell, its length $L_M(\tau + \Delta\tau)$ is

$$L_M(\tau + \Delta\tau) = L_M(\tau) \exp\left(\int_{\tau}^{\tau+\Delta\tau} (1 - f_P)g_M(R, B)dt\right) \tag{19}$$

From Eq. 9 and 6,

$$\frac{dP}{dt} = f_P g_M(R, B)M \sim \frac{f_P}{1 - f_P}\frac{dM}{dt}$$

and we get

$$P(\tau + \Delta\tau) = P(\tau) + \frac{f_P}{1 - f_P}\left(M(\tau + \Delta\tau) - M(\tau)\right)$$

where $M(\tau + \Delta\tau) = \sum L_M(\tau + \Delta\tau)$ is the sum of the lengths of all M cells.

To describe discrete death events, each H and M cell has a probability of $\delta_H\Delta\tau$ and $\delta_M\Delta\tau$ to die, respectively. This is simulated by assigning a random number between [0, 1] for each cell and those receive a random number less than $\delta_H\Delta\tau$ or $\delta_M\Delta\tau$ get eliminated. For surviving cells, if a cell's length ≥ 2, this cell will divide into two cells with half the original length.

Each cell has a probability of $P_{mut} = 0.002$ to acquire a mutation that changes each of its phenotype (Methods, Section 4). Without loss of generality, let's consider mutations in f_P. After mutation, f_P will be multiplied by $(1 + \Delta f_P)$, where Δf_P is determined as below.

First, a uniform random number u_1 is generated. If $u_1 \leq 0.5$, $\Delta f_P = -1$, which represents 50% chance of a null mutation ($f_P = 0$). If $0.5 < u_1 \leq 1$, Δf_P follows the distribution defined by Eq. 22 with $s_+(f_P) = 0.05$ for f_P-enhancing mutations and $s_-(f_P) = 0.067$ for f_P-diminishing mutations when epistasis is not considered (Methods, Section 4). In the simulation, Δf_P is generated via inverse transform sampling. Specifically, $C(\Delta f_P)$, the cumulative distribution function (CDF) of Δf_P , can be found by integrating Eq. 15 from -1 to Δf_P:

$$\begin{aligned} C(\Delta f_P) &= \int_{-1}^{\Delta f_P} \mu_{\Delta s}(x)dx \\ &= \begin{cases} \frac{s_-}{s_+ + s_-(1-e^{-1/s_-})}\left(\exp(\Delta f_P/s_-) - \exp(-1/s_-)\right) & \text{if } \Delta f_P \leq 0 \\ 1 - \frac{s_+}{s_+ + s_-(1-e^{-1/s_-})}\exp(-\Delta f_P/s_+) & \text{if } \Delta f_P \geq 0 \end{cases} \end{aligned} \tag{20}$$

The two parts of Eq. 20 overlap at $C(\Delta f_P = 0) = s_-(1 - e^{-1/s_-})/\left[s_+ + s_-(1 - e^{-1/s_-})\right]$.

In order to generate Δf_P satisfying the distribution in Eq. 15, a uniform random number u_2 between 0 and 1 is generated and we set $C(\Delta f_P) = u_2$. Inverting Eq. 20 yields

$$\Delta f_P = \begin{cases} s_- \ln\left(u_2(s_+ + s_-(1-e^{-1/s_-}))/s_- + e^{-1/s_-}\right) & u_2 \le \frac{s_-(1-e^{-1/s_-})}{s_+ + s_-(1-e^{-1/s_-})} \\ -s_+ \ln\left((1-u_2)(s_+ + s_-(1-e^{-1/s_-}))/s_+\right) & u_2 > \frac{s_-(1-e^{-1/s_-})}{s_+ + s_-(1-e^{-1/s_-})} \end{cases} \quad (21)$$

When epistasis is considered, $s_+(f_P) = s_{+init}/(1 + g \times (f_P/f_{P,init} - 1))$ and $s_-(f_P) = s_{-init} \times (1 + g \times (f_P/f_{P,init} - 1))$ are used in Eq. 21 to calculated Δf_P for each cell with different current f_P (Methods Section 6).

If for a certain f_P, $f_{P,mut} = f_P(1+\Delta f_P) > 1$, $f_{P,mut}$ is set to 1 (upper bound). In general, if a mutation increases or decreases the phenotypic parameter beyond its bound, the phenotypic parameter is set to the bound value.

The above growth-death/birth-mutation cycle is repeated from time 0 to T. Note that since the size of each M and H cell can be larger than 1, the integer numbers of M and H cells, I_M and I_H, are generally smaller than biomass M and H , respectively. At the end of T, the communities are sorted according to $P(T)$.

For community reproduction, we save the current random number generator state to generate random numbers for partitioning the Adult. When we do not fix total biomass or total cell number, we do the following. We select the Adult community with the highest function (or a randomly-chosen Adult community in control simulations). The fold by which this Adult will be diluted is $n_D = \lfloor (M(T) + H(T))/N_0 \rfloor$ where $N_0 = 100$ is the pre-set target for total biomass of a Newborn, and $\lfloor x \rfloor$ is the floor function that generates the largest integer that is smaller than x. $I_H + I_M$ random integers between 1 and n_D are uniformly generated so that each M and H cell is assigned a random integer between 1 and n_D. All cells assigned with the same random integer belong to the same Newborn. This generates n_D newborn communities. This partition regimen can be experimentally implemented by pipetting $1/n_D$ volume of an Adult community into a new well. If n_D is less than n_{tot} (the total number of communities under selection), all n_D newborn communities are kept. Then, we partition the Adult with the second highest function (or a random community in control simulations) to obtain an additional batch of n_D Newborns, and if this is enough, we will randomly pick from these a sufficient number of Newborns to obtain n_{tot} Newborns. The next cycle then begins.

To "fix" Newborn total biomass $N(0)$ to the target total biomass N_0, total biomass $N(0)$ is counted so that $N(0)$ comes closest to the target N_0 without exceeding it (otherwise, $P(T)$ may exceed the theoretical maximum). For example, suppose that a certain number of M and H cells have been sorted into a Newborn so that the total biomass is 98.6. If the next cell, either M or H, has a mass of 1.3, this cell goes into the community so that the total biomass is $98.6 + 1.3 = 99.9$. However, if a cell of mass 1.6 happens to be picked, this cell doesn't go into this community so that this Newborn has a total biomass of 98.6 and the cell of mass 1.6 goes to the next Newborn. Thus, each Newborn may not have exactly the biomass of N_0, but rather between $N_0 - 2$ and N_0. Experimentally, total biomass can be determined from the optical density (OD), or from the total fluorescence if cells are fluorescently labeled (bioRxiv). In most simulations we fix the total biomass of each Newborn because biomass $M(t)$ and $H(t)$ are the quantities used in Eqs. 6-10 and Eqs. 16-19. If a cell sorter can only track the number of cells (instead of also tracking cell size), we perform simulations where the we sort a total of $\lfloor N_0/1.5 \rfloor$ cells into each Newborn, assuming that the average biomass of an M or H cell is 1.5. We obtain the same conclusion, as shown in Figure 22 left panels.

To fix $\phi_M(0)$ (while allowing total biomass $N(0)$ to fluctuate), we generate Newborn communities so that $\phi_M(0) = \phi_M(T)$ of the selected Adult community from the previous cycle. Again, because each M and H has a biomass (or length) between 1 and 2, $\phi_M(0)$ of each Newborn community may not be exactly $\phi_M(T)$ of the selected Adult community. In the code, dilution fold n_D is calculated in the same fashion as mentioned above. $I_M(T)$ random integers between $[1, n_D]$ are then generated for each M cell. All M cells assigned the same random integer belong to the same Newborn community. A total biomass of $M(0)(1-\phi_M(T))/\phi_M(T)$ of H cells should be sorted into this Newborn community. In the code, H cells are randomly dispensed into each Newborn community until the total biomass of H comes closest to $M(0)(1-\phi_M(T))/\phi_M(T)$ without exceeding it. Again, because each H cell has a biomass between 1 and 2, the total biomass of H might not be exactly $M(0)(1-\phi_M(T))/\phi_M(T)$ but between $M(0)(1-\phi_M(T))/\phi_M(T) - 2$ and $M(0)(1-\phi_M(T))/\phi_M(T)$. We have also performed simulations where the ratio of M and H cell numbers in the Newborn community,

$I_M(0)/I_H(0)$, is set to $I_M(T)/I_H(T)$ of the Adult community, and obtain the same conclusion (Figure 22 center panels).

To fix both $N(0)$ and $\phi_M(0)$, we sort a total biomass of $N_0\phi_M(T)$ of M cells and a total biomass of $N_0(1-\phi_M(T))$ of H cells into each Newborn community. Here, $N_0 = 100$ is preset and $\phi_M(T)$ is measured from the selected Adult community of the previous cycle. In the code, to form a Newborn community, M cells are randomly picked from the Adult community until the total biomass of M comes closest to $N(0)\phi_M(T)$ without exceeding it. H cells are sorted similarly. Because each M and H cells has a length between 1 and 2, the biomass of M can vary between $N(0)\phi_M(T) - 2$ and $N(0)\phi_M(T)$ and the biomass of H can vary between $N(0)(1-\phi_M(T)) - 2$ and $N(0)(1-\phi_M(T))$. Although such a partition scheme does not completely eliminate variations in species composition among Newborn communities, such variations are sufficiently small so that community selection can improve $\overline{f}_P(T)$. We have also performed simulations where the total number of cells is set to $\lfloor N_0/1.5 \rfloor$ with $\lfloor N_0\varphi_M(T)/1.5 \rfloor$ M cells and $\lfloor N_0(1-\varphi_M(T))/1.5 \rfloor$ H cells where $\varphi_M(T) = I_M(T)/(I_M(T)+I_H(T))$ is calculated from the numbers instead of biomass of M and H cells. We obtain the same conclusion (Figure 22, right panels).

6 Modeling epistasis on f_P

Epistasis, where the effect of a new mutation depends on prior mutations ("genetic background"), is known to affect evolutionary dynamics. Epistatic effects have been quantified in various ways. Experiments on virus, bacterium, yeast, and proteins have demonstrated that for two mutations that are both deleterious or random, viable double mutants experience epistatic effects that are nearly symmetrically distributed around a value near zero [87, 88, 89, 90, 91]. In other words, a significant fraction of mutation pairs show no epistasis, and a small fraction show positive or negative epistasis (i.e. a double mutant displays a stronger or weaker phenotype than expected from additive effects of the two single mutants). Epistasis between two beneficial mutations can vary from being predominantly negative [88] to being symmetrically distributed around zero [89]. Furthermore, a beneficial mutation tends to confer a lower beneficial effect if the background already has high fitness ("diminishing returns") [92, 89, 93].

A mathematical model by Wiser et al. incorporates diminishing returns epistasis [86]. In this model, beneficial mutations of advantage s in the ancestral background are exponentially distributed with probability density $\alpha \exp(-\alpha s)$, where $1/\alpha > 0$ is the mean advantage. After a mutation with advantage s has occurred, the mean advantage of the next mutation would be reduced to $1/[\alpha(1+gs)]$, where $g > 0$ is the "diminishing returns parameter". Wiser et al. estimates $g \approx 6$. This model quantitatively explains the fitness dynamics of evolving *E. coli* populations.

Based on experimental and theoretical literature, we model epistasis on f_P in the following manner. Let the relative mutation effect on f_P be $\Delta f_P = (f_{P,mut} - f_P)/f_P \geq -1$. Then, $\mu(\Delta f_P,\ f_P)$, the probability density function of Δf_P at the current f_P value, is described by a form similar to Eq. 15:

$$\mu(\Delta f_P,\ f_P) = \begin{cases} \frac{1}{s_+(f_P)+s_-(f_P)(1-\exp(-1/s_-(f_P)))} \exp(-\Delta f_P/s_+(f_P)) & \text{if } \Delta f_P \geq 0 \\ \frac{1}{s_+(f_P)+s_-(f_P)(1-\exp(-1/s_-(f_P)))} \exp(\Delta f_P/s_-(f_P)) & \text{if } -1 < \Delta f_P < 0 \end{cases} \quad (22)$$

Here, $s_+(f_P)$ and $s_-(f_P)$ are respectively the mean Δf_P for enhancing and diminishing mutations at current f_P. $s_+(f_P) = s_{+init}/(1 + g \times (f_P/f_{P,init} - 1))$, where $f_{P,init}$ is the f_P of the initial background (e.g. 0.13 for mono-adapted Manufacturer), s_{+init} is the mean enhancing Δf_P occurring in the initial background, and $0 < g < 1$ is the epistatic factor. Similarly, $s_-(f_P) = s_{-init} \times (1 + g \times (f_P/f_{P,init} - 1))$ is the mean $|\Delta f_P|$ for diminishing mutations at current f_P. In the initial background since $f_P = f_{P,init}$, we have $s_+(f_P) = s_{+init}$ and $s_-(f_P) = s_{-init}$ where $s_{+init} = 0.050$ and $s_{-init} = 0.067$ (Figure 13). For subsequent mutations, mean Δf_P is modified by epistatic factor g. Consistent with diminishing returns principle, if current $f_P > f_{P,init}$, then a new enhancing mutation becomes less likely and a new diminishing mutation becomes more likely (ensured by $g > 0$). Similarly, if current $f_P < f_{P,init}$, then a new enhancing mutation becomes more likely and a diminishing mutation becomes less likely (ensured by $0 < g < 1$). Thus, as f_P approaches 1, $s_+(f_P)$ decreases and $s_-(f_P)$ increases (Figure 14). That is, enhancing mutations become less likely, and diminishing mutations become more likely. Conversely as f_P approaches 0, the opposite is true ($s_+(f_P)$ increases and $s_-(f_P)$ decreases, Figure 14). In summary, our model captures not only diminishing returns of enhancing mutations, but also our understanding of mutational effects on protein stability [72].

7 Pathology of two alternative definitions of community function

For a given Newborn community, we define community function as $P(T)$, the total amount of Product at maturation time T. Below, we describe the pathology of alternative definitions of community function.

Let's consider a simpler case where groups of Manufacturers are selected for high P, and cell death is negligible. We have

$$\frac{dM}{dt} = (1 - f_P) g_M M \tag{23}$$

$$\frac{dP}{dt} = f_P g_M M \tag{24}$$

where biomass growth rate g_M is a function of B and R. When M and H compete for Resource, g_M also depends implicitly on f_P because f_P affects M:H and therefore B and R.

Since from Eq. 23 and 24

$$\frac{dM}{(1 - f_P)dt} = \frac{dP}{f_P dt}$$

we have

$$P(T) = \frac{f_P}{1 - f_P} \left(M(T) - M(0) \right) \approx \frac{f_P}{1 - f_P} M(T)$$

if $M(T) \gg M(0)$. This is true if T is long enough for cells to double at least three or four times.

If we define community function as $P(T)/M(T)$ (total Product normalized against M biomass in Adult community), $P(T)/M(T) \approx \frac{f_P}{1-f_P}$. Under this definition, higher $\frac{f_P}{1-f_P}$ or higher f_P always leads to higher community function, and higher f_P in turn leads to M extinction (Figure 3).

If the community function is instead defined as $P(T)/M(0)$, then

$$\frac{P(T)}{M(0)} \approx \frac{f_P}{1 - f_P} \frac{M(T)}{M(0)} = \frac{f_P}{1 - f_P} \exp\left((1 - f_P) \int_T g_M dt \right) \tag{25}$$

From Eq. 25, at a fixed f_P, $\frac{P(T)}{M(0)}$ increases as $\int_T g_M dt$ increases. $\int_T g_M dt$ increases as $\phi_M(0)$ decreases, since the larger fraction of Helper, the faster the accumulation of Byproduct and the larger $\int_T g_M dt$ (Figure 27B). Thus, we end up selecting communities with small $\phi_M(0)$ (Figure 12). This means that Manufactures could get lost during community reproduction, and community selection then fails.

For groups or communities with a certain $\int_T g_M dt$, we can calculate f_P optimal for community function from Eq. 25 by setting

$$\frac{dP(T)}{df_p} = M(0) \frac{d}{df_p} \left[\frac{f_P}{1 - f_P} \exp\left((1 - f_P) \int_T g_M dt \right) \right] = 0$$

We have $\frac{1}{(1-f_P)^2} \exp\left((1 - f_P) \int_T g_M dt \right) - \frac{f_P}{1-f_P} \int_T g_M dt \exp\left((1 - f_P) \int_T g_M dt \right) = 0$, or $1/\int_T g_M dt = f_P(1 - f_P)$.

If $\int_T g_M dt \gg 1$, f_P is very small, and the optimal f_P for $P(T)$ is

$$f_P^* \approx \left(\int_T g_M dt \right)^{-1} \tag{26}$$

8 Identify optimal $P(T)$

For a Newborn community with total biomass $N(0) = 100$, we fix growth parameters of M and H to upper bounds, and calculate $P(T)$ under various f_P and $\phi_M(0)$. Since both numbers range between 0 and 1, we calculate $P(T, f_P = 0.01 \times i, \phi_M(0) = 0.01 \times j)$ for integers i and j between 1 and 99. There is a global maximum for $P(T)$ when $i = 41$ and $j = 54$ (see the accompanying article). Therefore the optimal f_P and $\phi_M(0)$ combination for a Newborn community with $N(0) = 100$ are 0.41 and 0.54, respectively.

9 Pathology associated with community reproduction via fixed-fold dilution

If Resource is unlimited, then there is no competition between H and M. According to Eq. 25, $P(T)$ increases linearly with $M(0)$. $P(T)$ also increases with $H(0)$, since higher $H(0)$ leads to higher Byproduct and consequently higher $\int_T g_M dt$ in the exponent. Newborn communities can vary significantly in their $N(0)$ due to stochastic fluctuations (with a standard deviation of $\sqrt{N_0}$). Thus each cycle, communities with larger $N(0)$ (instead of higher f_p) will get selected. With unlimited Resource, the size of an Adult community has no upper bound. After a fixed-fold dilution, $N(0)$ also has no upper bound. In comparison, the average f_p of different Newborns do not vary nearly as much (Figure 8).

Acknowledgment

We thank the following for discussions: members of the Shou group, Lin Chao (UCSD), Maitreya Dunham (UW Seattle), Corina Tarnita (Princeton), and Harmit Malik (Fred Hutch). We thank Alex Yuan (UW Seattle), Chichun Chen (Indiana University Bloomington), Bill Hazelton, Samuel Hart, David Skelding, and Doug Jackson for feedback on the manuscript. This research was supported by the High Performance Computing Shared Resource of the Fred Hutch (P30 CA015704).

Supplementary Figures

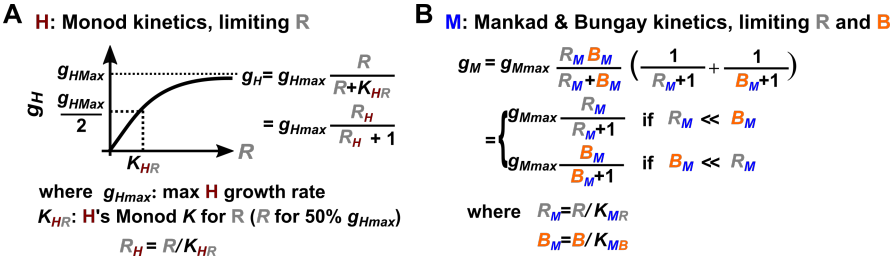

Figure 9: **Figure 2-figure supplement 1.** (**A**) H growth follows Monod kinetics, reaching half maximal growth rate when $R = K_{HR}$. (**B**) M growth follows dual-substrate Mankad and Bungay kinetics. When Resource R is in great excess ($R_M \gg B_M$) or Byproduct B is in great excess ($B_M \gg R_M$), we recover mono-substrate Monod kinetics (**A**).

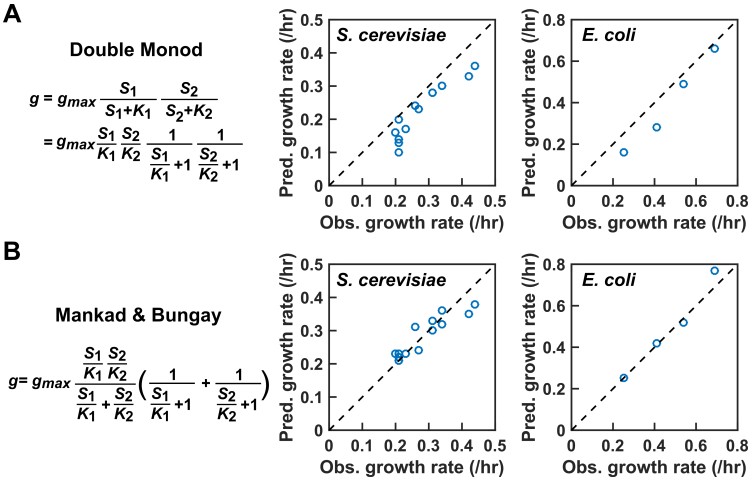

Figure 10: **Figure 2-figure supplement 2. A comparison of dual-substrate models.** Suppose that cell growth rate depends on each of the two substrates S_1 and S_2 in a Monod-like, saturable fashion. When S_2 is in excess, the S_1 at which half maximal growth rate is achieved is K_1. When S_1 is in excess, the S_2 at which half maximal growth rate is achieved is K_2. (**A**) In the "Double Monod" model, growth rate depends on the two limiting substrates in a multiplicative fashion. In the model proposed by Mankad and Bungay (**B**), growth rate takes a different form. In both models, when one substrate is in excess, growth rate depends on the other substrate in a Monod-fashion. However, differences exist. For example, when $\frac{S_1}{K_1} = \frac{S_2}{K_2} = 1$, the growth rate is predicted to be $g_{max}/2$ by Mankad & Bunday model, and $g_{max}/4$ by the Double Monod model. Mankad and Bungay model outperforms the Double Monod model in describing experimental data of *S. cerevisiae* and *E. coli* growing on low glucose and low nitrogen. The figures are plotted using data from Ref. [43].

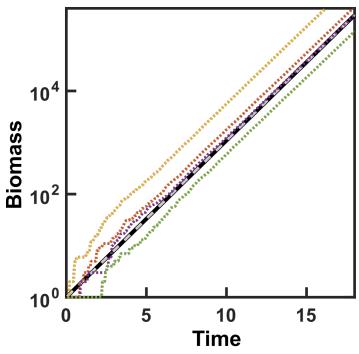

Figure 11: **Figure 2-figure supplement 3. A comparison of birth models.** We modeled exponential biomass growth in excess metabolites. Thick black line: analytical solution with biomass growth rate (0.7/time unit). Grey dashed line: simulation assuming that biomass increases exponentially at 0.7/time unit and that cell division occurs upon reaching a biomass threshold, an assumption used in our model. Color dotted lines: simulations assuming that cell birth occurs at a probability equal to the birth rate multiplied with the length of simulation time step ($\Delta\tau = 0.05$). When a cell birth occurs, biomass increases discretely by 1, resulting in step-wise increase in color dotted lines at early time.

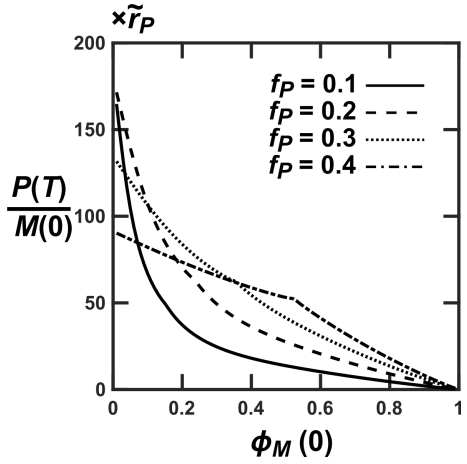

Figure 12: **Figure 2-figure supplement 4.** The pathology of artificial community selection if community function is defined as $P(T)/M(0)$. Over the range of f_P where M and H can coexist, $P(T)/M(0)$ increases as $\phi_M(0)$ decreases.

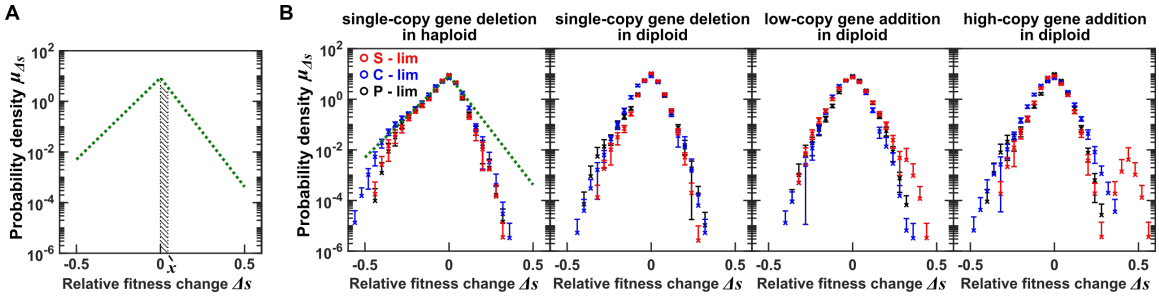

Figure 13: **Figure 4 - Figure Supplement 1. Probability density functions of changes in relative fitness due to mutations ($\mu_{\Delta s}(\Delta s)$).** (**A**) Suppose that green line represents the probability density function of Δs, the relative fitness change in mutants. Then the probability $P(0 \leq \Delta s \leq x)$ is the area of the shaded region. (**B**) We derived $\mu_{\Delta s}(\Delta s)$ from the Dunham lab data [52] where bar-coded mutant strains were competed under sulfate-limitation (red), carbon-limitation (blue), or phosphate-limitation (black). Error bars represent uncertainty $\delta\mu_{\Delta s}$ (the lower error bar is omitted if the lower estimate is negative). In the leftmost panel, green lines show non-linear least squared fitting of data to Eq. 15 using all three sets of data. Note that data with larger uncertainty are given less weight, and thus deviate more from the fitting lines. For an exponentially-distributed probability density function, the average fitness effect is 1/slope. From the green line on the right side, we obtain the average effect of enhancing mutations $s_+ = 0.050 \pm 0.002$, and from the green line on the left side, we obtain the average effect of diminishing mutations $s_- = 0.067 \pm 0.003$.

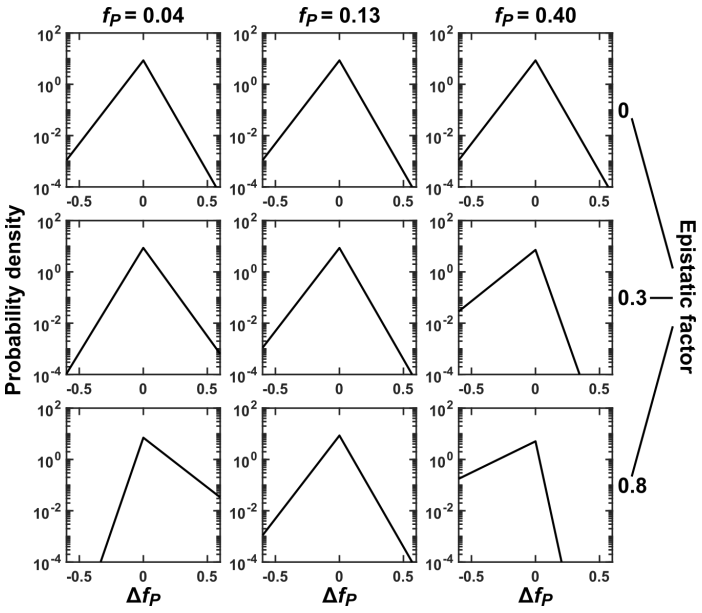

Figure 14: **Figure 4-Figure Supplement 2. Mutation effects under epistasis.** Distribution of mutation effects at different current f_P values are plotted. (Top) When there is no epistasis, distribution of mutational effects on f_P ($\triangle f_P$) are identical regardless of current f_P. (Middle and Bottom) With epistasis (see Methods Section 6 for definition of epistasis factor), mutational effects on f_P depend on the current value of f_P. If current f_P is low (left), enhancing mutations are more likely to occur while diminishing mutations are less likely to occur; if current f_P is high (right), the opposite is true.

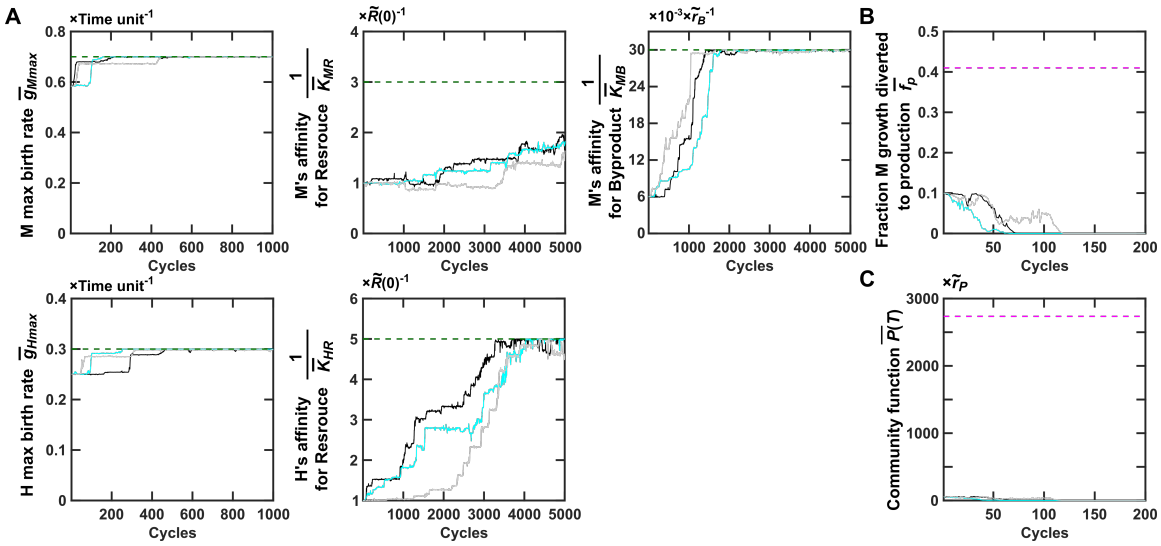

Figure 15: **Figure 5-Figure Supplement 1. Community function declines to zero in the absence of community selection**. Without community selection, natural selection favors fast growers with improved maximal growth rates and improved affinities for nutrients (**A**). Consequently, f_P (**B**) and thus $P(T)$ (**C**) decrease to zero. Maximal growth rates of H and M (g_{Hmax} and g_{Mmax}), H's affinity for Resource $1/K_{HR}$, and M's affinity for Byproduct $1/K_{MB}$ rapidly improve to their respective upper bounds, while M's affinity for Resource $1/K_{MR}$ improves more slowly. This is consistent with M's growth being more limited by Byproduct. $\overline{P}(T)$ is averaged across the two randomly selected Adult communities. $\overline{g}_{Mmax}$, $\overline{g}_{Hmax}$, and $\overline{f}_P$ are obtained by averaging within each randomly-selected Adult community and then averaging across the two randomly-selected Adult communities. $K_{SpeciesMetabolite}$ are averaged within each randomly-selected Adult community, then across the two randomly-selected Adults, and finally inverted to represent average affinity. Green dashed lines: upper bounds of phenotypes; Magenta dashed lines: f_P optimal for community function and maximal $P(T)$ when all five growth parameters are fixed at their upper bounds and $\phi_M(0)$ is also optimal for $P(T)$. Note different x axis scales. Black, cyan, and gray curves show three independent simulations.

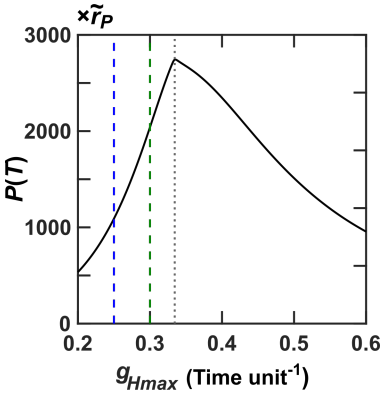

Figure 16: **Figure 5-Figure Supplement 2. Improving maximal growth rate of Helper g_{Hmax} does not necessarily improve community function**. We have chosen the ancestral (blue dashed line) and the evolutionary upper bound (green dashed line) of g_{Hmax} such that improving g_{Hmax} improves community function. Suppose we have chosen ancestral g_{Hmax} at the grey dotted line, then higher g_{Hmax} would lower community function. The black curve is obtained by numerically integrating Eqs. 6-10 at different g_{Hmax} values where f_P is set to 0.4 and all growth parameters except for g_{Hmax} are set to their respective upper bounds. $N(0)$ is 100, and $\phi_M(0)$ is 0.7 (close to steady-state value).

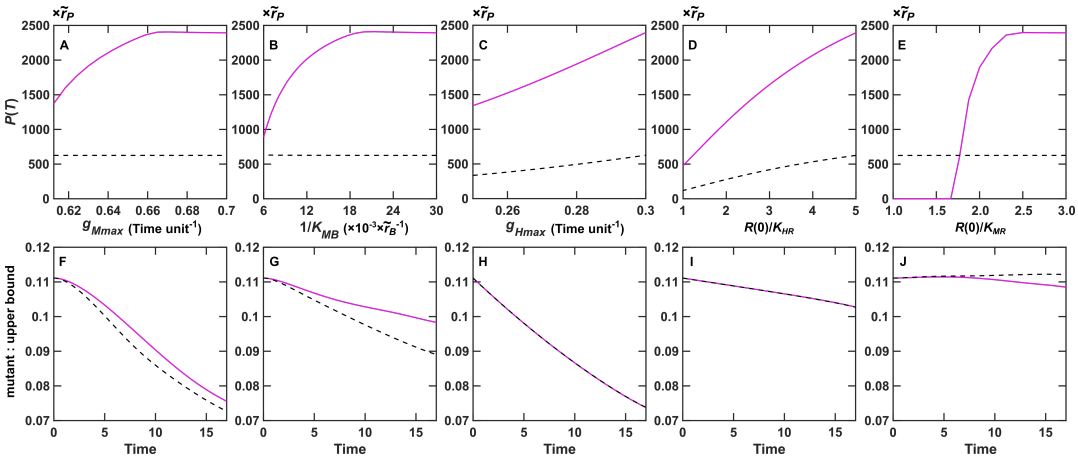

Figure 17: **Figure 5-Figure Supplement 3. Improving maximal growth rates and nutrient affinities generally, but do not always, improve individual fitness and community function.** In all figures, solid and dashed lines respectively represent dynamics when $f_P = 0.41$ (optimal for community function if all growth parameters are fixed at their upper bounds; Figure 6A) and $f_P = 0.13$ (optimal for M monoculture production when Byproduct is in excess; Figure 6B). (A-D) Community function increases as g_{Mmax}, $1/K_{MB}$, g_{Hmax} or $1/K_{HR}$ increases when other growth parameters are fixed at their upper bounds. For example, In (A), all growth parameters except for g_{Mmax} are at their upper bounds, and for each combination of g_{Mmax} and f_P, the steady-state $\phi_{M,SS}$ is calculated using equations in Methods Section 1. This steady-state $\phi_{M,SS}$ is then used to calculate $P(T)$. (F-I) respectively show that mutant individuals with g_{Mmax}, $1/K_{MB}$, g_{Hmax} or $1/K_{HR}$ 10% lower than the upper bound have lower fitness. For example in (F), a Newborn community has 70 M and 30 H. 90% of M have upper bound $g_{Mmax} = 0.7$ ("upper bound"). 10% of M have $g_{Mmax} = 0.63$, 10% less than the upper bound ("mutant"). Other growth parameters are all at upper bounds. The ratio between mutant and upper bound drops over maturation time, indicating that M cells with mutant (lower) maximal growth rate have lower fitness. (E, J) When $f_P = 0.13$ (black dashed line) but not when $f_P = 0.41$ (magenta line), increasing M's affinity for Resource ($1/K_{MR}$) slightly decreases both $P(T)$ and individual fitness.

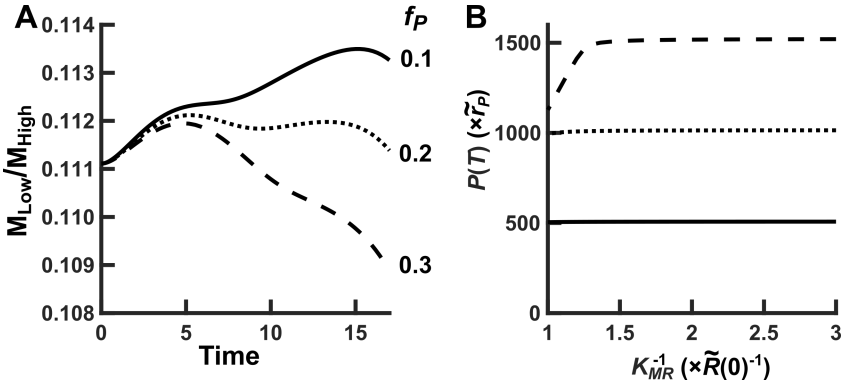

Figure 18: **Figure 5-Figure Supplement 4. At low f_P, higher $1/K_{MR}$ can lead to reduced M growth rate. (A)** The ratio between M_{Low} with low affinity for R ($K_{MR}^{-1} = 2.5\widetilde{R}(0)^{-1}$) and M_{High} with high affinity for R ($K_{MR}^{-1} = 3\widetilde{R}(0)^{-1}$) when their f_P is equal to 0.1 (solid line), 0.2 (dotted line) and 0.3 (dashed line) are plotted over one maturation cycle. **(B)** $P(T)$ improves over increasing affinity K_{MR}^{-1} when f_P is 0.1 (solid line), 0.2 (dotted line) and 0.3 (dashed line). The dependence of $P(T)$ on K_{MR}^{-1} is rather weak for low f_P. For example, when K_{MR}^{-1} increases from $\widetilde{R}(0)^{-1}$ to $3\widetilde{R}(0)^{-1}$, $P(T)$ increases only by 2% and 0.6% for $f_P = 0.2$ and $f_P = 0.1$, respectively.

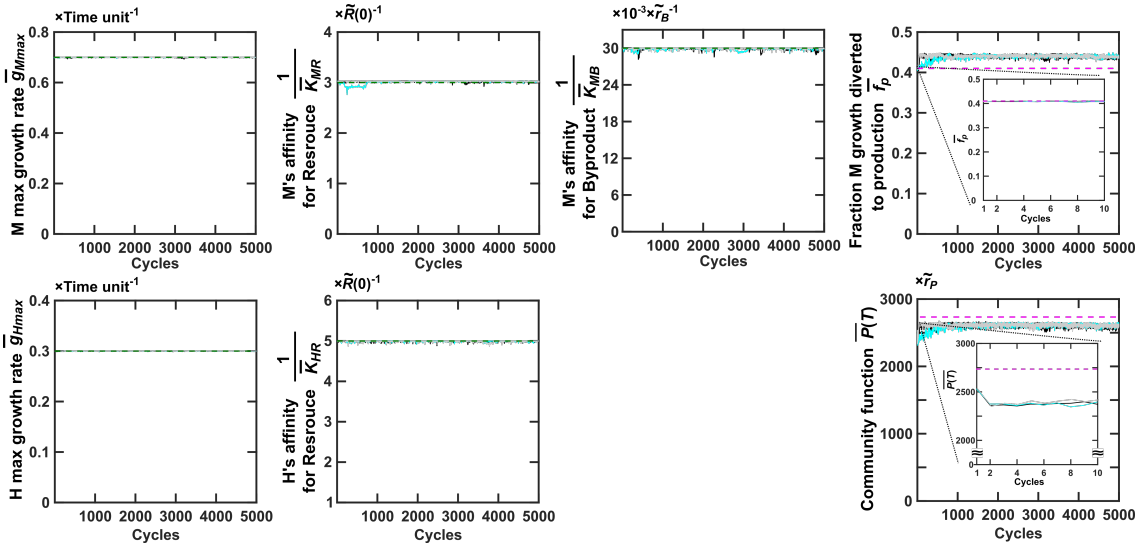

Figure 19: **Figure 6-Figure Supplement 1. Local optimality of community function $P^*(T)$.** We start each Newborn community with total biomass $N(0)$=100, all five growth parameters at their upper bounds, and $f_P^* = 0.41$ and $\phi_M^*(0) = 0.54$ to achieve $P^*(T)$. We then allow all five growth parameters and f_P to mutate while applying community selection. To ensure effective community selection (see the last section of Results), during community reproduction, we fix $N(0)$ to 100, and assign $\phi_M(0)$ to $\phi_M(T)$ of the previous cycle. We find that all five growth parameters remain at their respective evolutionary upper bounds. At the end of the first cycle (Cycle=1 in insets), even though $\overline{f}_P$ has not changed, $\overline{P}(T)$ has already declined from the magenta dashed line. This is because $\phi_M(0)$ has changed via ecological interactions to 0.73, close to the steady state ϕ_M instead of the optimal $\phi_M^*(0)$ of 0.54. Later, over hundreds of cycles, $\overline{f}_P$ gradually increases, which increases $\overline{P}(T)$. However, $\overline{P}(T)$ is still below maximal. This is because species composition gravitates toward steady state $\phi_{M,SS}$ which deviates from what is required for $P^*(T)$. See the accompanying article for further discussions. $\bar{g}_{Mmax}$, $\bar{g}_{Hmax}$, and $\overline{f}_P$ are obtained by averaging within each selected Adult community and then averaging across the two selected Adults. $K_{SpeciesMetabolite}$ are similarly averaged, and then inverted to represent average affinity. Green dashed lines: upper bounds of phenotypes; Magenta dashed lines: f_P^* and $P^*(T)$ when all five growth parameters are fixed at their upper bounds and $\phi_M(0) = \phi_M^*(0)$.

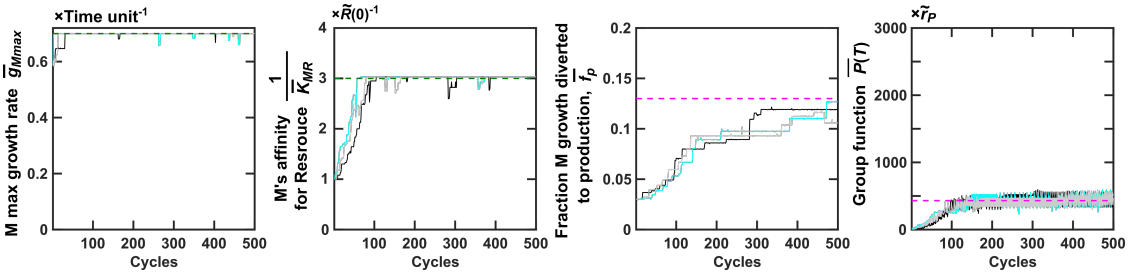

Figure 20: **Figure 6-Figure Supplement 2. Selection dynamics of M mono-species groups**. Phenotypes averaged over selected groups are plotted. Because Byproduct is in excess, K_{MB} terms are no longer relevant in equations (Figure 10, $R_M \ll B_M$). upper bounds of g_{Mmax} and $1/K_{MR}$ are marked with green dashed lines. Magenta lines mark maximal f_P and $P(T)$ when g_{Mmax} and $1/K_{MR}$ are fixed at their upper bounds and when Byproduct is in excess.

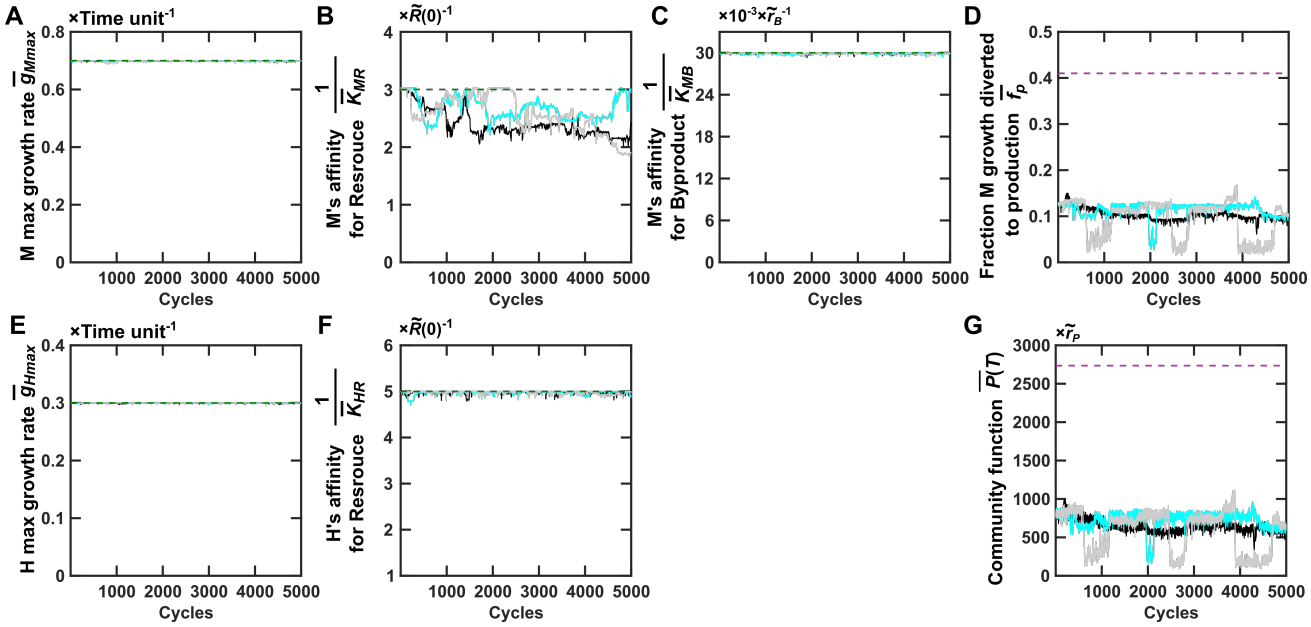

Figure 21: . **Figure 7-Figure supplement 1. Selection dynamics of communities of mono-adapted H and M when allowing all parameters to vary**. g_{Mmax}, g_{Hmax}, $1/K_{MB}$ and $1/K_{HR}$ remain mostly constant during community selection because mutants with lower-than-maximal values are weeded out by natural selection as well as community selection. However, $1/K_{MR}$ decreases slightly because at low f_P, M with a lower affinity for R (lower$1/K_{MR}$) slight improves individual fitness while slightly decreasing community function (Figure 18). $\bar{g}_{Mmax}$, $\bar{g}_{Hmax}$, and $\overline{f}_P$ are obtained by averaging within each selected Adult community and then averaging across the two selected Adults. $K_{SpeciesMetabolite}$ are similarly averaged, and then inverted to represent average affinity. $\overline{P}(T)$ are averaged across the two selected Adults. Black, cyan and gray curves are three independent simulations. Green dashed lines indicate upper bounds for growth parameters. Magenta dashed lines: f_P optimal for community function and optimal $P(T)$ when all five growth parameters are fixed at their upper bounds and $\phi_M(0)$ is also optimal for $P(T)$.

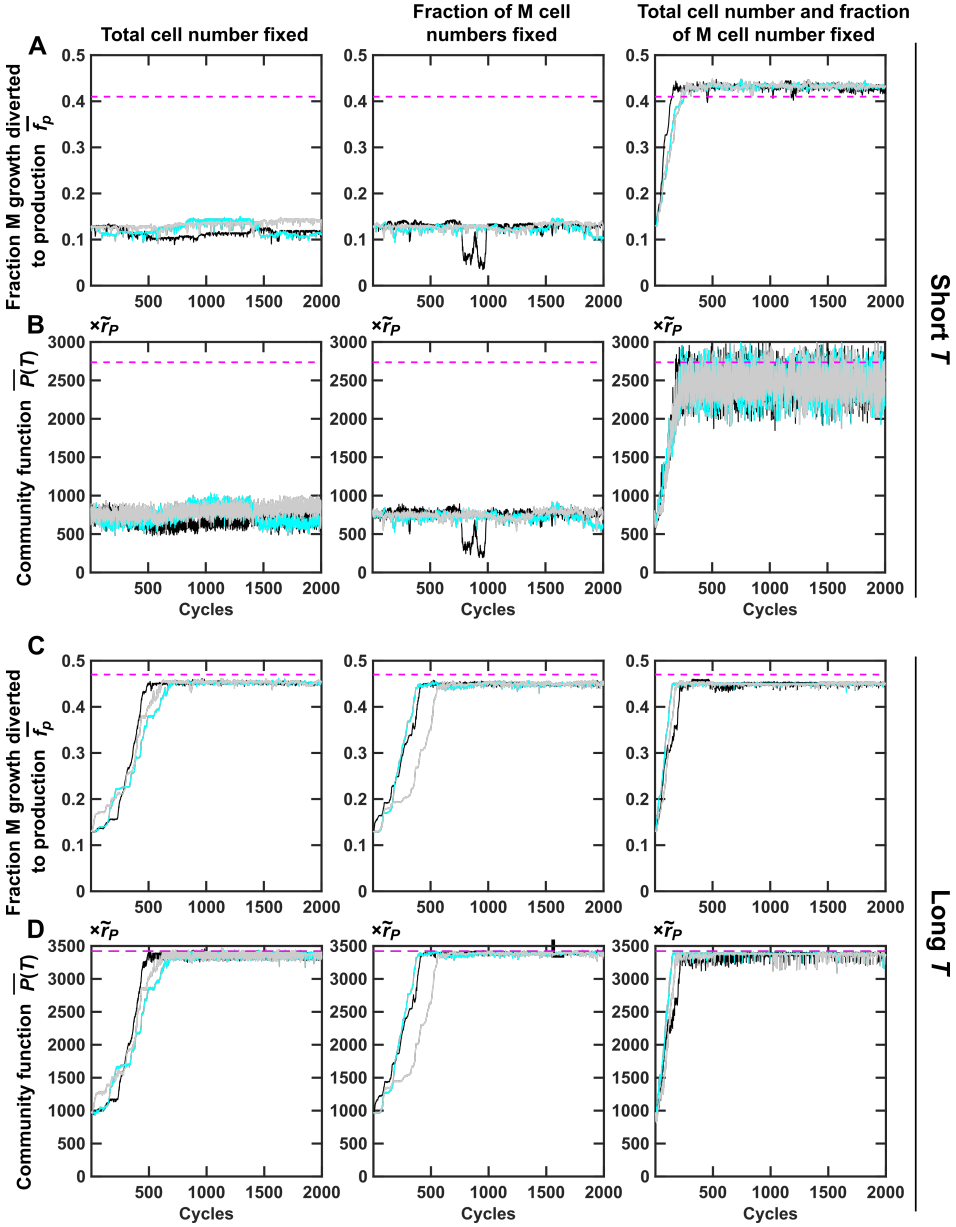

Figure 22: **Figure 7-Figure Supplement 2. Fixing H and M cell numbers (instead of biomass) during community reproduction allows short-T selection regimen to improve community function.** For left panels, the total cell number is fixed to $\lfloor N_0/1.5 \rfloor$. For center panels, the ratio between M and H cell numbers are fixed to $I_M(T)/I_H(T)$, where $I_M(T)$ and $I_H(T)$ are the number of M and H cells in the selected Adult community, respectively. For right panels, the total cell numbers are fixed to $\lfloor N_0/1.5 \rfloor$ and the ratio between M and H cell numbers are fixed to $I_M(T)/I_H(T)$. See Methods Section 5 for details of simulating community reproduction. $\overline{f}_P$ is averaged across members of each selected community, and subsequently averaged across the two selected communities. Community function $\overline{P}(T)$ is averaged across the two selected communities. Black, cyan and gray curves are three independent simulations.

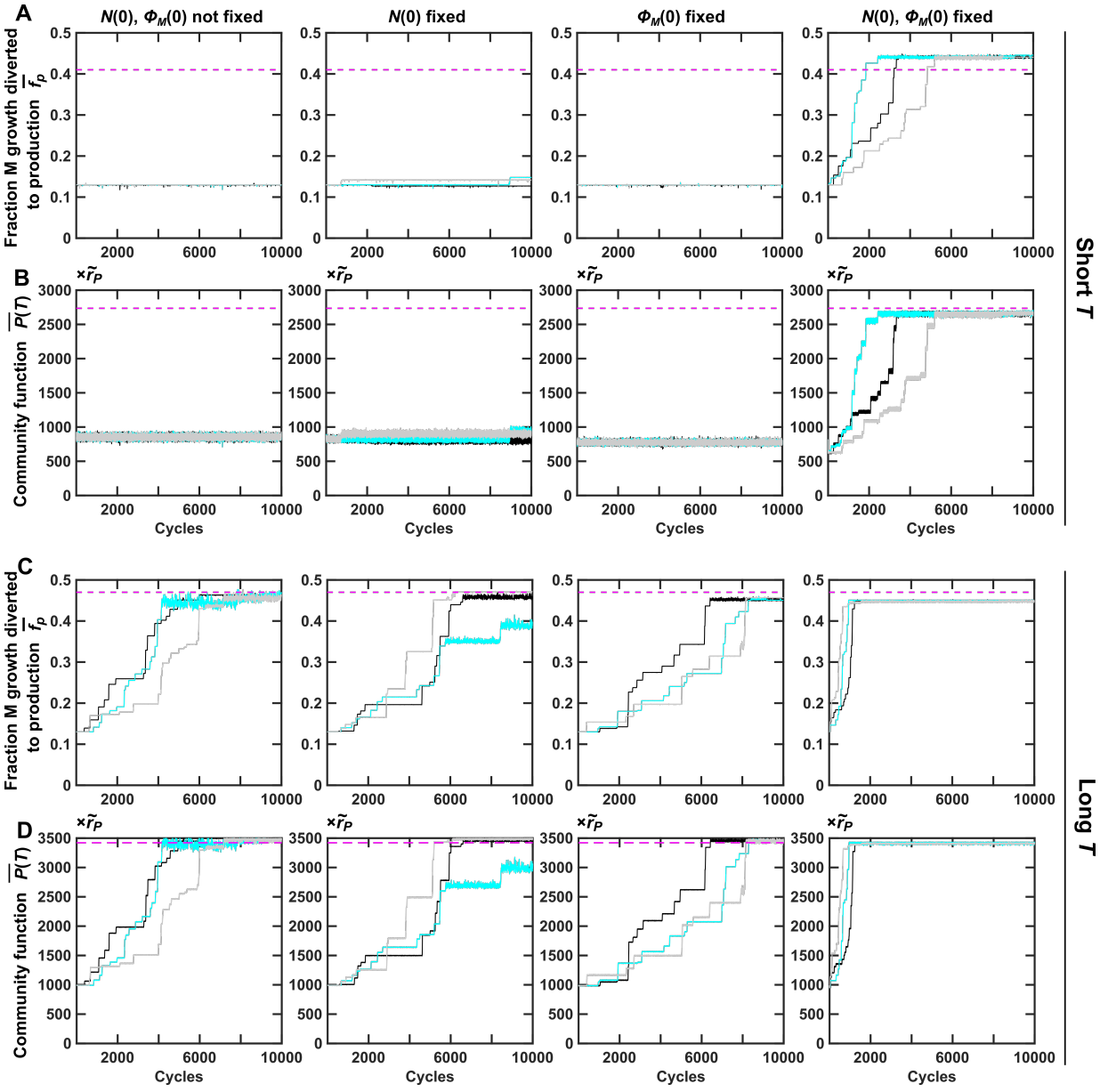

Figure 23: **Figure 7-Figure Supplement 3. Evolution dynamics of selected Adult communities at a low mutation rate of 2×10^{-5} per cell per generation.** (**A, B**) At short maturation time ($T = 17$, Resource is not exhausted in an average community), fixing both $N(0)$ and $\phi_M(0)$ is required for community function to improve. (**C, D**) At long maturation time ($T = 20$, Resource is exhausted in an average community), community function improves without needing to fix $N(0)$ or $\phi_M(0)$. When both are fixed, community function improves even faster. $\overline{f}_P$ is averaged across members of each selected community, and subsequently averaged across the two selected communities. Community function $\overline{P}(T)$ is averaged across the two selected communities. Black, cyan and gray curves are three independent simulations. At this low mutation rate, because the population size of a community never exceeds 10^4, a mutation occurs on average every 5 cycles, resulting in step-wise improvement in both $\overline{f}_P(T)$ and $\overline{P}(T)$.

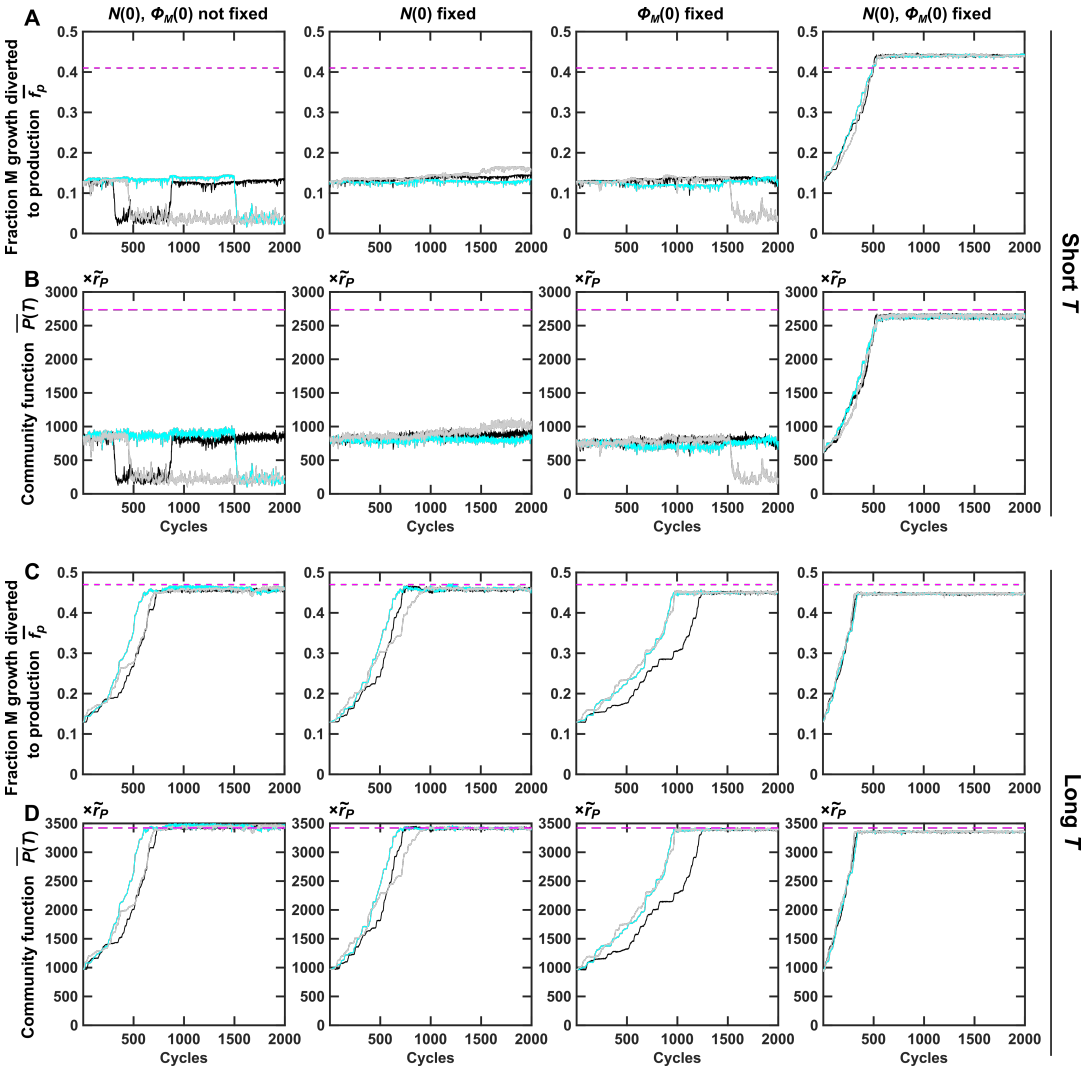

Figure 24: **Figure 7-Figure Supplement 4. Evolution dynamics of selected Adult communities under a different distribution of mutation effect.** Here, the distribution of mutation effects is specified by Eq. 15 where $s_+ = s_- = 0.02$ are constants. $\overline{f}_P$ is averaged across members of each selected community, and subsequently averaged across the two selected communities. Community function $\overline{P}(T)$ is averaged across the two selected communities. Black, cyan and gray curves are three independent simulations.

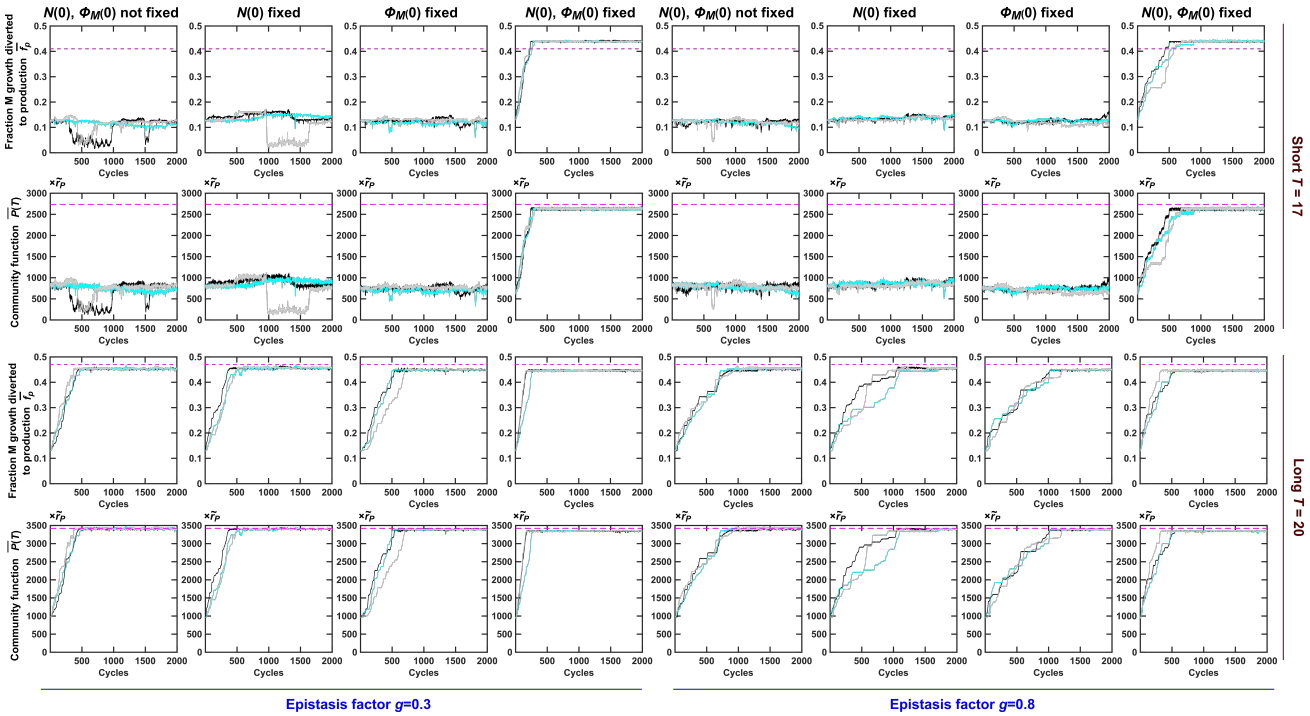

Figure 25: **Figure 7-Figure Supplement 5. Evolution dynamics of selected Adult communities when epistasis is considered.** When we incorporate different epistasis strengths (epistasis factor of 0.3 and 0.8), we obtain essentially the same conclusions as when epistasis is not considered (Figure 7). $\overline{f}_P$ is averaged across members of each selected community, and subsequently averaged across the two selected communities. Community function $\overline{P}(T)$ is averaged across the two selected communities. Black, cyan and gray curves are three independent simulations.

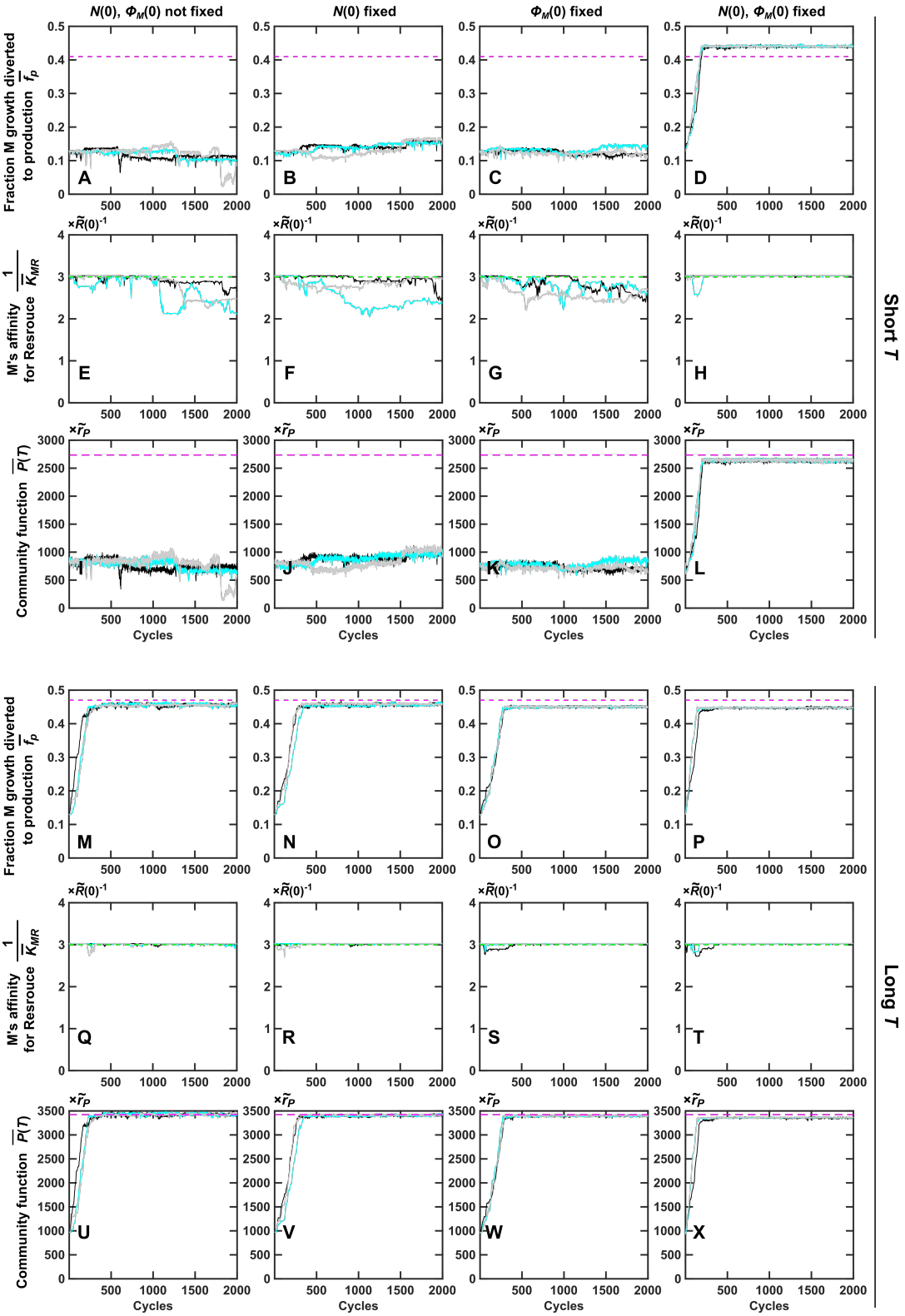

Figure 26: **Figure 7-Figure Supplement 6. Evolution dynamics of selected Adult communities when both f_P and K_{MR} are allowed to mutate.** Green dashed lines indicate upper bounds for growth parameters. Magenta dashed lines: f_P optimal for community function and optimal $P(T)$ when all five growth parameters are fixed at their upper bounds and $\phi_M(0)$ is also optimal for $P(T)$. $\overline{f}_P$ is averaged across members of each selected community, and subsequently averaged across the two selected communities. $\overline{K}_{MR}$ is similarly averaged, and then inverted to represent average affinity. Community function $\overline{P}(T)$ is averaged across the two selected communities. Black, cyan and gray curves are three independent simulations.

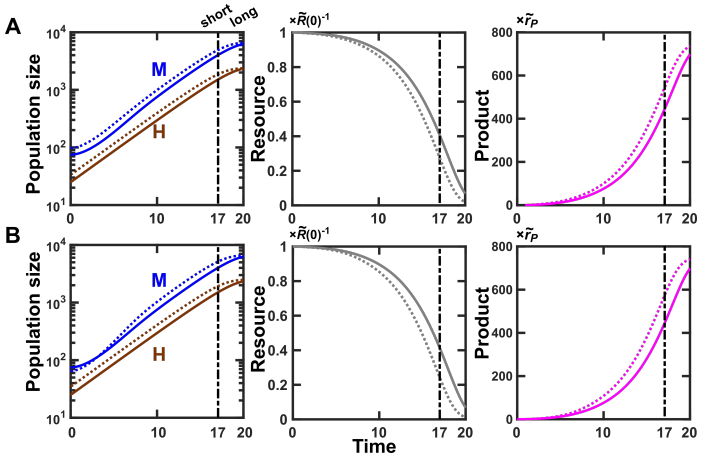

Figure 27: **Figure 8-Figure Supplement 1. Variations in community function can arise from non-heritable variations in Newborn compositions.** An average Newborn community (solid lines) has a total biomass of 100 with 75% M. (A) A "lucky" Newborn community (dotted lines), by stochastic fluctuations, has a total biomass of 130 with 75% M. Even though the two communities share identical $f_P = 0.1$, the Newborn with 130 total biomass has its M growing to a larger size (left), depleting more Resource (middle), and making more Product (right) if T is short. (B) A "lucky" Newborn community (dotted lines), by stochastic fluctuations, has 100 total biomass with 65% M. Even though the two communities share identical $f_P = 0.1$, the Newborn with lower $\phi_M(0)$ (dotted) has its M enjoying a shorter growth lag and growing to a larger size (left), depleting more Resource (middle), and making more Product (right) if T is short. In both cases, the difference between lucky (dotted) and average (solid) communities is diminished at longer T ($T = 20$) compared to shorter T ($T = 17$, dash dot line).

References

[1] Trevor D. Lawley, Simon Clare, Alan W. Walker, Mark D. Stares, Thomas R. Connor, Claire Raisen, David Goulding, Roland Rad, Fernanda Schreiber, Cordelia Brandt, Laura J. Deakin, Derek J. Pickard, Sylvia H. Duncan, Harry J. Flint, Taane G. Clark, Julian Parkhill, and Gordon Dougan. Targeted restoration of the intestinal microbiota with a simple, defined bacteriotherapy resolves relapsing Clostridium difficile disease in mice. *PLoS pathogens*, 8(10):e1002995, 2012.

[2] Souichiro Kato, Shin Haruta, Zong Jun Cui, Masaharu Ishii, and Yasuo Igarashi. Effective cellulose degradation by a mixed-culture system composed of a cellulolytic Clostridium and aerobic non-cellulolytic bacteria. *FEMS Microbiology Ecology*, 51(1):133–142, 2004.

[3] Stefanie Widder, Rosalind J. Allen, Thomas Pfeiffer, Thomas P. Curtis, Carsten Wiuf, William T. Sloan, Otto X. Cordero, Sam P. Brown, Babak Momeni, Wenying Shou, Helen Kettle, Harry J. Flint, Andreas F. Haas, Béatrice Laroche, Jan-Ulrich Kreft, Paul B. Rainey, Shiri Freilich, Stefan Schuster, Kim Milferstedt, Jan R. van der Meer, Tobias Groβkopf, Jef Huisman, Andrew Free, Cristian Picioreanu, Christopher Quince, Isaac Klapper, Simon Labarthe, Barth F. Smets, Harris Wang, Isaac Newton Institute Fellows, and Orkun S. Soyer. Challenges in microbial ecology: building predictive understanding of community function and dynamics. *The ISME Journal*, March 2016. 00001.

[4] Stephen R. Lindemann, Hans C. Bernstein, Hyun-Seob Song, Jim K. Fredrickson, Matthew W. Fields, Wenying Shou, David R. Johnson, and Alexander S. Beliaev. Engineering microbial consortia for controllable outputs. *The ISME Journal*, 10(9):2077–2084, September 2016.

[5] Jian Zhou, Qian Ma, Hong Yi, Lili Wang, Hao Song, and Ying-Jin Yuan. Metabolome profiling reveals metabolic cooperation between Bacillus megaterium and Ketogulonicigenium vulgare during induced swarm motility. *Applied and Environmental Microbiology*, 77(19):7023–7030, October 2011. 00038.

[6] R. E. Wheatley. The consequences of volatile organic compound mediated bacterial and fungal interactions. *Antonie van Leeuwenhoek*, 81(1-4):357–364, December 2002. 00123.

[7] Kwang-sun Kim, Soohyun Lee, and Choong-Min Ryu. Interspecific bacterial sensing through airborne signals modulates locomotion and drug resistance. *Nature Communications*, 4:1809, 2013.

[8] Matthew F Traxler, Jeramie D Watrous, Theodore Alexandrov, Pieter C Dorrestein, and Roberto Kolter. Interspecies interactions stimulate diversification of the Streptomyces coelicolor secreted metabolome. *mBio*, 4(4), 2013.

[9] A. Crameri, E. A. Whitehorn, E. Tate, and W. P. Stemmer. Improved green fluorescent protein by molecular evolution using DNA shuffling. *Nature Biotechnology*, 14(3):315–319, March 1996.

[10] Manfred T. Reetz and José Daniel Carballeira. Iterative saturation mutagenesis (ISM) for rapid directed evolution of functional enzymes. *Nature Protocols*, 2(4):891–903, April 2007.

[11] Eric T. Boder, Katarina S. Midelfort, and K. Dane Wittrup. Directed evolution of antibody fragments with monovalent femtomolar antigen-binding affinity. *Proceedings of the National Academy of Sciences*, 97(20):10701–10705, September 2000.

[12] W. D. Hamilton. The genetical evolution of social behaviour I and II. *Journal of Theoretical Biology*, 7(1):1–52, July 1964.

[13] John Maynard Smith. Group Selection and Kin Selection. *Nature*, 201(4924):1145–1147, March 1964.

[14] Sewall Wright. Tempo and Mode in Evolution: A Critical Review. *Ecology*, 26(4):415–419, 1945.

[15] George R. Price. Selection and Covariance. *Nature*, 227(5257):520–521, August 1970. 01240.

[16] Michael J. Wade. A Critical Review of the Models of Group Selection. *The Quarterly Review of Biology*, 53(2):101–114, June 1978. ArticleType: research-article / Full publication date: Jun., 1978 / Copyright © 1978 The University of Chicago Press.

[17] William M Muir. Group selection for adaptation to multiple-hen cages: selection program and direct responses. *Poultry Science*, 75(4):447–458, 1996.

[18] David C. Queller and Joan E. Strassmann. Kin Selection and Social Insects. *BioScience*, 48(3):165–175, March 1998.

[19] Michael J Wade. An experimental study of kin selection. *Evolution*, pages 844–855, 1980.

[20] Arne Traulsen and Martin A. Nowak. Evolution of cooperation by multilevel selection. *Proceedings of the National Academy of Sciences*, 103(29):10952–10955, July 2006.

[21] L. Lehmann, L. Keller, S. West, and D. Roze. Group selection and kin selection: Two concepts but one process. *Proc Natl Acad Sci USA*, 104(16):6736–6739, April 2007.

[22] Benjamin Kerr. Theoretical and experimental approaches to the evolution of altruism and the levels of selection. *Experimental Evolution: Concepts, Methods, and Applications of Selection Experiments*, pages 585–630, 2009. 00006.

[23] Herwig Bachmann, Frank J Bruggeman, Douwe Molenaar, Filipe Branco dos Santos, and Bas Teusink. Public goods and metabolic strategies. *Current Opinion in Microbiology*, 31:109–115, June 2016. 00000.

[24] Katrin Hammerschmidt, Caroline J. Rose, Benjamin Kerr, and Paul B. Rainey. Life cycles, fitness decoupling and the evolution of multicellularity. *Nature*, 515(7525):75–79, November 2014.

[25] Martin A. Nowak. Five Rules for the Evolution of Cooperation. *Science*, 314(5805):1560–1563, December 2006.

[26] C. J. Goodnight and L. Stevens. Experimental studies of group selection: what do they tell us about group selection in nature? *The American Naturalist*, 150 Suppl 1:S59–79, July 1997.

[27] Herwig Bachmann, Martin Fischlechner, Iraes Rabbers, Nakul Barfa, Filipe Branco dos Santos, Douwe Molenaar, and Bas Teusink. Availability of public goods shapes the evolution of competing metabolic strategies. *Proceedings of the National Academy of Sciences of the United States of America*, 110(35):14302–14307, August 2013.

[28] John S Chuang, Olivier Rivoire, and Stanislas Leibler. Simpson's paradox in a synthetic microbial system. *Science (New York, N.Y.)*, 323(5911):272–275, January 2009.

[29] Wenying Shou. Acknowledging selection at sub-organismal levels resolves controversy on pro-cooperation mechanisms. *eLife*, page e10106, December 2015.

[30] R C Lewontin. The Units of Selection. *Annual Review of Ecology and Systematics*, 1(1):1–18, 1970.

[31] D. S. Wilson. A theory of group selection. *Proceedings of the National Academy of Sciences*, 72(1):143–146, January 1975.

[32] Michael E Gilpin. *Group selection in predator-prey communities*, volume 9. Princeton University Press, 1975.

[33] J. Maynard Smith. Group Selection. *The Quarterly Review of Biology*, 51(2):277–283, June 1976.

[34] Michael Doebeli, Yaroslav Ispolatov, and Burt Simon. Towards a mechanistic foundation of evolutionary theory. *eLife*, 6:e23804, February 2017.

[35] L. Chao and B.R. Levin. Structured habitats and the evolution of anticompetitor toxins in bacteria. *Proc Natl Acad Sci U S A*, 78(10):6324–8, October 1981.

[36] Hywel T. P. Williams and Timothy M. Lenton. Artificial selection of simulated microbial ecosystems. *Proceedings of the National Academy of Sciences*, 104(21):8918–8923, May 2007. 00036.

[37] William Swenson, David Sloan Wilson, and Roberta Elias. Artificial ecosystem selection. *Proceedings of the National Academy of Sciences*, 97:9110–9114, 2000.

[38] W. Swenson, J. Arendt, and D.S. Wilson. Artificial selection of microbial ecosystems for 3-chloroaniline biodegradation. *Environ Microbiol*, 2(5):564–71, October 2000.

[39] Jeremy J. Minty, Marc E. Singer, Scott A. Scholz, Chang-Hoon Bae, Jung-Ho Ahn, Clifton E. Foster, James C. Liao, and Xiaoxia Nina Lin. Design and characterization of synthetic fungal-bacterial consortia for direct production of isobutanol from cellulosic biomass. *Proceedings of the National Academy of Sciences*, 110(36):14592–14597, September 2013. 00024 PMID: 23959872.

[40] Kang Zhou, Kangjian Qiao, Steven Edgar, and Gregory Stephanopoulos. Distributing a metabolic pathway among a microbial consortium enhances production of natural products. *Nature biotechnology*, 2015.

[41] Hyun-Dong Shin, Shara McClendon, Trinh Vo, and Rachel R. Chen. Escherichia coli Binary Culture Engineered for Direct Fermentation of Hemicellulose to a Biofuel. *Applied and Environmental Microbiology*, 76(24):8150–8159, December 2010. 00000.

[42] Shen-Long Tsai, Garima Goyal, and Wilfred Chen. Surface Display of a Functional Minicellulosome by Intracellular Complementation Using a Synthetic Yeast Consortium and Its Application to Cellulose Hydrolysis and Ethanol Production. *Applied and Environmental Microbiology*, 76(22):7514–7520, November 2010.

[43] T Mankad and HR Bungay. Model for microbial growth with more than one limiting nutrient. *Journal of biotechnology*, 7(2):161–166, 1988.

[44] Sattar Taheri-Araghi, Serena Bradde, John T. Sauls, Norbert S. Hill, Petra Anne Levin, Johan Paulsson, Massimo Vergassola, and Suckjoon Jun. Cell-Size Control and Homeostasis in Bacteria. *Current Biology*, 25(3):385–391, February 2015.

[45] Babak Momeni, Kristen A Brileya, Matthew W Fields, and Wenying Shou. Strong inter-population cooperation leads to partner intermixing in microbial communities. *eLife*, 2:e00230, 2013. 00000.

[46] Jeffrey E Barrick, Dong Su Yu, Sung Ho Yoon, Haeyoung Jeong, Tae Kwang Oh, Dominique Schneider, Richard E Lenski, and Jihyun F Kim. Genome evolution and adaptation in a long-term experiment with escherichia coli. *Nature*, 461(7268):1243, 2009.

[47] Toon Swings, Bram Van den Bergh, Sander Wuyts, Eline Oeyen, Karin Voordeckers, Kevin J Verstrepen, Maarten Fauvart, Natalie Verstraeten, and Jan Michiels. Adaptive tuning of mutation rates allows fast response to lethal stress in escherichia coli. *eLife*, 6(22939), 2017.

[48] Clifford Zeyl and J Arjan GM DeVisser. Estimates of the rate and distribution of fitness effects of spontaneous mutation in saccharomyces cerevisiae. *Genetics*, 157(1):53–61, 2001.

[49] Rafael Sanjuán, Andrés Moya, and Santiago F Elena. The distribution of fitness effects caused by single-nucleotide substitutions in an rna virus. *Proceedings of the National Academy of Sciences of the United States of America*, 101(22):8396–8401, 2004.

[50] Karen S Sarkisyan, Dmitry A Bolotin, Margarita V Meer, Dinara R Usmanova, Alexander S Mishin, George V Sharonov, Dmitry N Ivankov, Nina G Bozhanova, Mikhail S Baranov, Onuralp Soylemez, et al. Local fitness landscape of the green fluorescent protein. *Nature*, 533(7603):397–401, 2016.

[51] Dominika M Wloch, Krzysztof Szafraniec, Rhona H Borts, and Ryszard Korona. Direct estimate of the mutation rate and the distribution of fitness effects in the yeast saccharomyces cerevisiae. *Genetics*, 159(2):441–452, 2001.

[52] Celia Payen, Anna B Sunshine, Giang T Ong, Jamie L Pogachar, Wei Zhao, and Maitreya J Dunham. High-throughput identification of adaptive mutations in experimentally evolved yeast populations. *PLoS genetics*, 12(10):e1006339, 2016.

[53] Adam James Waite, Caroline Cannistra, and Wenying Shou. Defectors Can Create Conditions That Rescue Cooperation. *PLoS Comput Biol*, 11(12):e1004645, December 2015. 00000.

[54] Richard E Lenski and Michael Travisano. Dynamics of adaptation and diversification: a 10,000-generation experiment with bacterial populations. *Proceedings of the National Academy of Sciences*, 91(15):6808–6814, 1994.

[55] Adam James Waite and Wenying Shou. Adaptation to a new environment allows cooperators to purge cheaters stochastically. *Proceedings of the National Academy of Sciences*, 109(47):19079–19086, 2012.

[56] Paul B Rainey and Katrina Rainey. Evolution of cooperation and conflict in experimental bacterial populations. *Nature*, 425(6953):72, 2003.

[57] Rafael U Ibarra, Jeremy S Edwards, and Bernhard O Palsson. Escherichia coli k-12 undergoes adaptive evolution to achieve in silico predicted optimal growth. *Nature*, 420(6912):186, 2002.

[58] Thomas Egli. *Nutrition, microbial*. Oxford: Elsevier Academic Press, 2009.

[59] R Haselkorn. Heterocysts. *Annual Review of Plant Physiology*, 29(1):319–344, June 1978.

[60] Ronald Aylmer Fisher. *The genetical theory of natural selection: a complete variorum edition*. Oxford University Press, 1999.

[61] Nick Colegrave. Sex releases the speed limit on evolution. *Nature*, 420(6916):664–666, 2002.

[62] Philip J Gerrish and Richard E Lenski. The fate of competing beneficial mutations in an asexual population. *Genetica*, 102:127, 1998.

[63] Stephen T Chisholm, Gitta Coaker, Brad Day, and Brian J Staskawicz. Host-microbe interactions: shaping the evolution of the plant immune response. *Cell*, 124(4):803–814, 2006.

[64] Ruth E Ley, Micah Hamady, Catherine Lozupone, Peter J Turnbaugh, Rob Roy Ramey, J Stephen Bircher, Michael L Schlegel, Tammy A Tucker, Mark D Schrenzel, Rob Knight, et al. Evolution of mammals and their gut microbes. *Science*, 320(5883):1647–1651, 2008.

[65] Kevin R Foster, Jonas Schluter, Katharine Z Coyte, and Seth Rakoff-Nahoum. The evolution of the host microbiome as an ecosystem on a leash. *Nature*, 548(7665):43, 2017.

[66] Luc De Vuyst, Raf Callewaert, and Kurt CrabbÃ©. Primary metabolite kinetics of bacteriocin biosynthesis by Lactobacillus amylovorus and evidence for stimulation of bacteriocin production under unfavourable growth conditions. *Microbiology*, 142(4):817–827, 1996.

[67] Babak Momeni, Kristen A Brileya, Matthew W Fields, and Wenying Shou. Strong inter-population cooperation leads to partner intermixing in microbial communities. *eLife*, 2, January 2013.

[68] Wenying Shou, Sri Ram, and Jose M. G. Vilar. Synthetic cooperation in engineered yeast populations. *Proceedings of the National Academy of Sciences of the United States of America*, 104(6):1877–1882, February 2007. 00137.

[69] Melanie JI Müller, Beverly I Neugeboren, David R Nelson, and Andrew W Murray. Genetic drift opposes mutualism during spatial population expansion. *Proceedings of the National Academy of Sciences*, 111(3):1037–1042, 2014.

[70] Kai Zhuang, Goutham N Vemuri, and Radhakrishnan Mahadevan. Economics of membrane occupancy and respiro-fermentation. *Molecular systems biology*, 7(1):500, 2011.

[71] Joan B Peris, Paulina Davis, José M Cuevas, Miguel R Nebot, and Rafael Sanjuán. Distribution of fitness effects caused by single-nucleotide substitutions in bacteriophage f1. *Genetics*, 185(2):603–609, 2010.

[72] Adrian WR Serohijos and Eugene I Shakhnovich. Merging molecular mechanism and evolution: theory and computation at the interface of biophysics and evolutionary population genetics. *Current opinion in structural biology*, 26:84–91, 2014.

[73] Adam Eyre-Walker and Peter D Keightley. The distribution of fitness effects of new mutations. *Nature reviews. Genetics*, 8(8):610, 2007.

[74] Michael A Stiffler, Doeke R Hekstra, and Rama Ranganathan. Evolvability as a function of purifying selection in tem-1 β-lactamase. *Cell*, 160(5):882–892, 2015.

[75] John W Drake. A constant rate of spontaneous mutation in dna-based microbes. *Proceedings of the National Academy of Sciences*, 88(16):7160–7164, 1991.

[76] Gregory I. Lang and Andrew W. Murray. Estimating the Per-Base-Pair Mutation Rate in the Yeast Saccharomyces cerevisiae. *Genetics*, 178(1):67–82, January 2008.

[77] Sasha F Levy, Jamie R Blundell, Sandeep Venkataram, Dmitri A Petrov, Daniel S Fisher, and Gavin Sherlock. Quantitative evolutionary dynamics using high-resolution lineage tracking. *Nature*, 519(7542):181, 2015.

[78] Maureen E Hillenmeyer, Eula Fung, Jan Wildenhain, Sarah E Pierce, Shawn Hoon, William Lee, Michael Proctor, Robert P St Onge, Mike Tyers, Daphne Koller, et al. The chemical genomic portrait of yeast: uncovering a phenotype for all genes. *Science*, 320(5874):362–365, 2008.

[79] Lília Perfeito, Lisete Fernandes, Catarina Mota, and Isabel Gordo. Adaptive mutations in bacteria: high rate and small effects. *Science*, 317(5839):813–815, 2007.

[80] John H Gillespie. Molecular evolution over the mutational landscape. *Evolution*, 38(5):1116–1129, 1984.

[81] H Allen Orr. The distribution of fitness effects among beneficial mutations. *Genetics*, 163(4):1519–1526, 2003.

[82] Marianne Imhof and Christian Schlötterer. Fitness effects of advantageous mutations in evolving escherichia coli populations. *Proceedings of the National Academy of Sciences*, 98(3):1113–1117, 2001.

[83] Rees Kassen and Thomas Bataillon. Distribution of fitness effects among beneficial mutations before selection in experimental populations of bacteria. *Nature genetics*, 38(4):484, 2006.

[84] Darin R Rokyta, Paul Joyce, S Brian Caudle, and Holly A Wichman. An empirical test of the mutational landscape model of adaptation using a single-stranded dna virus. *Nature genetics*, 37(4):441, 2005.

[85] Darin R Rokyta, Craig J Beisel, Paul Joyce, Martin T Ferris, Christina L Burch, and Holly A Wichman. Beneficial fitness effects are not exponential for two viruses. *Journal of molecular evolution*, 67(4):368, 2008.

[86] Michael J Wiser, Noah Ribeck, and Richard E Lenski. Long-term dynamics of adaptation in asexual populations. *Science*, 342(6164):1364–1367, 2013.

[87] Lukasz Jasnos and Ryszard Korona. Epistatic buffering of fitness loss in yeast double deletion strains. *Nature genetics*, 39(4):550, 2007.

[88] Rafael Sanjuán, Andrés Moya, and Santiago F Elena. The contribution of epistasis to the architecture of fitness in an rna virus. *Proceedings of the National Academy of Sciences of the United States of America*, 101(43):15376–15379, 2004.

[89] Aisha I Khan, Duy M Dinh, Dominique Schneider, Richard E Lenski, and Tim F Cooper. Negative epistasis between beneficial mutations in an evolving bacterial population. *Science*, 332(6034):1193–1196, 2011.

[90] Santiago F Elena and Richard E Lenski. Test of synergistic interactions among deleterious mutations in bacteria. *Nature*, 390(6658):395, 1997.

[91] Carlos L Araya, Douglas M Fowler, Wentao Chen, Ike Muniez, Jeffery W Kelly, and Stanley Fields. A fundamental protein property, thermodynamic stability, revealed solely from large-scale measurements of protein function. *Proceedings of the National Academy of Sciences*, 109(42):16858–16863, 2012.

[92] Hsin-Hung Chou, Hsuan-Chao Chiu, Nigel F Delaney, Daniel Segrè, and Christopher J Marx. Diminishing returns epistasis among beneficial mutations decelerates adaptation. *Science*, 332(6034):1190–1192, 2011.

[93] Sergey Kryazhimskiy, Daniel P Rice, Elizabeth R Jerison, and Michael M Desai. Global epistasis makes adaptation predictable despite sequence-level stochasticity. *Science*, 344(6191):1519–1522, 2014.